What can we learn from the nuclear ground state densities?

ECT* Trento Workshop
"Nuclear Physics at the edge of stability"
July 4, 2022 Trento Italy

H. Sagawa, RIKEN/University of Aizu

1. Introduction
2. Ground state correlations in the ground state densities
3. Trajectory in 2D-plot of IS vs IV density in ^{48}Ca and ^{208}Pb and Symmetry energy
3. IV density in ^{40}Ca and Isospin Symmetry Breaking Interactions
4. Summary and Future Perspectives

Physical Review C **102**, 064307 (2020)

Physics Letters B829 137072 (April, 2022)

Nuclear ground state density

Experiments:
Elastic electron scattering: charge density => proton density
Proton and neutron elastic scattering: neutron density
Parity violation electron scattering: weak density =>neutron density

Theory:
Hartree-Fock (Hartree) model: Skyrme, RMF
HF-BCS, HF-Bogolyubov models
Beyond mean field models:
Partcle-vibration model
HF+ground state correlations
Ab initio model: shell model, coupled cluster model, self-consistent Green's function

Examples: EoS parameters from nuclear observables

Isovector properties (e.g. $S(\rho)$) are thought to be well determined by the **neutron skin thickness** ($\Delta r_{np} \equiv \langle r_n^2 \rangle^{1/2} - \langle r_p^2 \rangle^{1/2}$) **of a heavy nucleus such as ^{208}Pb)**:

Macroscopic model: $\Delta r_{np} \sim \frac{1}{12} \frac{(N-Z)}{A} \frac{R}{J} L \quad (L \propto p_0^{neut})$

^{208}Pb

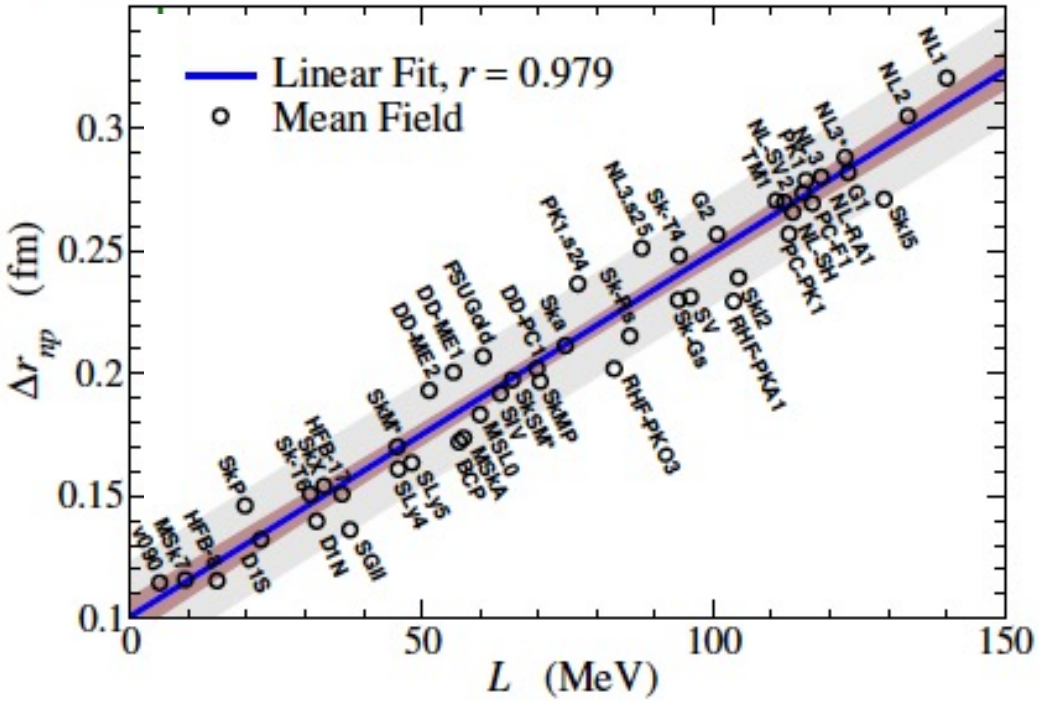

X. Roca-Maza

Physical Review Letters **106**, 252501 (2011)

Micorscopic models (EDFs) confirm such a relation

However the experimental precision and accuracy needed in the measurment of this property is very challenging nowadays.

Polarized proton elastic experiments for neutron density distributions
By Zenihiro et al.. RCNP experiments -> RIBF for exotic nuclei

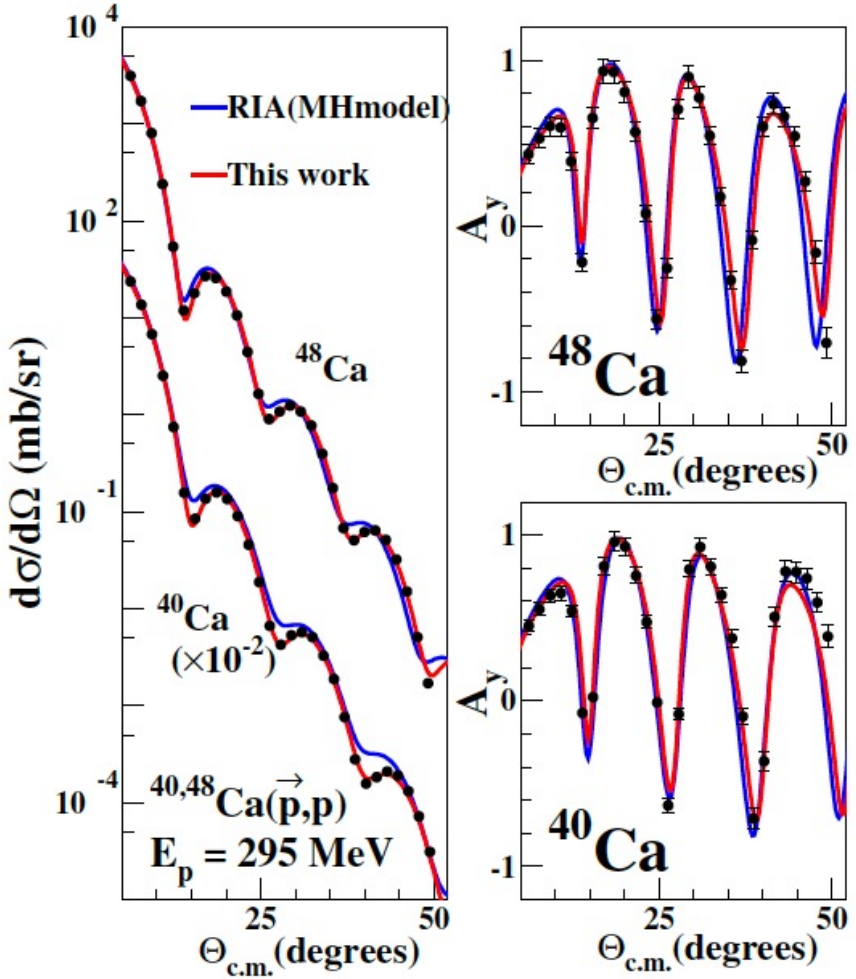

FIG. 1. Differential cross sections and analyzing powers for polarized proton elastic scattering from ^{40,48}Ca at 295 MeV. Blue and red lines are from the MH model and the result of the best-fit in this analysis, respectively.

Charge density=electron scatterings

Neutron density=>Relativistic Impulse approximation for proton elastic scatterings

$$F_{ch}(q) = F_p(q)G_E^p(q^2) + F_n(q)G_E^n(q^2) + F_{SO}(q), \quad (1)$$

where F_{ch}, $F_{p(n)}$, and $G_E^{p(n)}$ are the nuclear charge, the point-proton (neutron), and the Sachs single-nucleon electric form factors, respectively.

$$F_{SO}(q) \approx \frac{l(2j+1)(G_E^n(q^2) - 2G_M^n(q^2))}{4m^2}\mathcal{F}\left\{\frac{\partial(r\rho_n^l(r))}{r^2\partial r}\right\}, \quad (2)$$

$$(F_i(q) \equiv \mathcal{F}\{\rho_i(r)\} = \int \rho_i(r)\exp(i\boldsymbol{q}\cdot\boldsymbol{r})d\boldsymbol{r}),$$

The red hatched areas show
the standard error envelopes due to the experimental statistical and systematic errors only. The blue cross-hatched areas are shown to visualize the maximum uncertainty of the present method as well as the experimental errors.

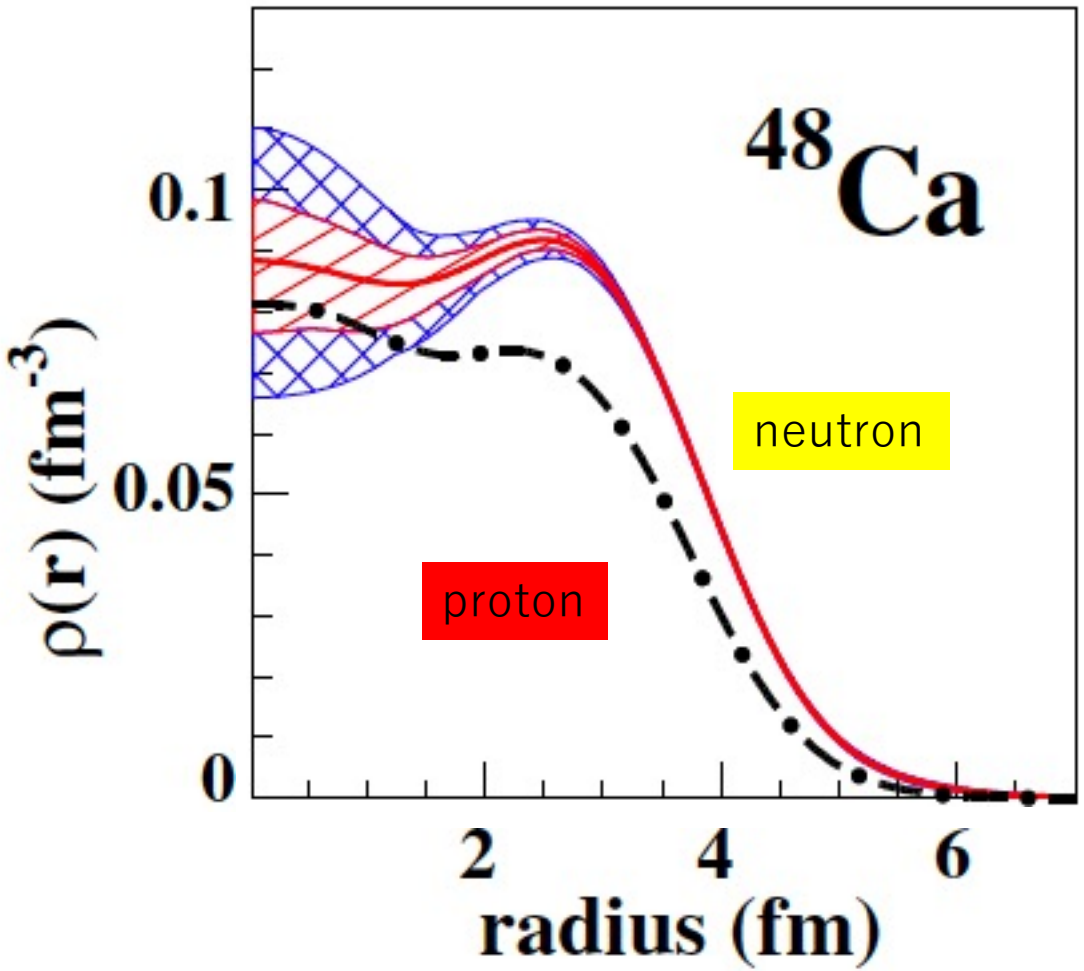

J. Zenihiro et al., preprint (2020)

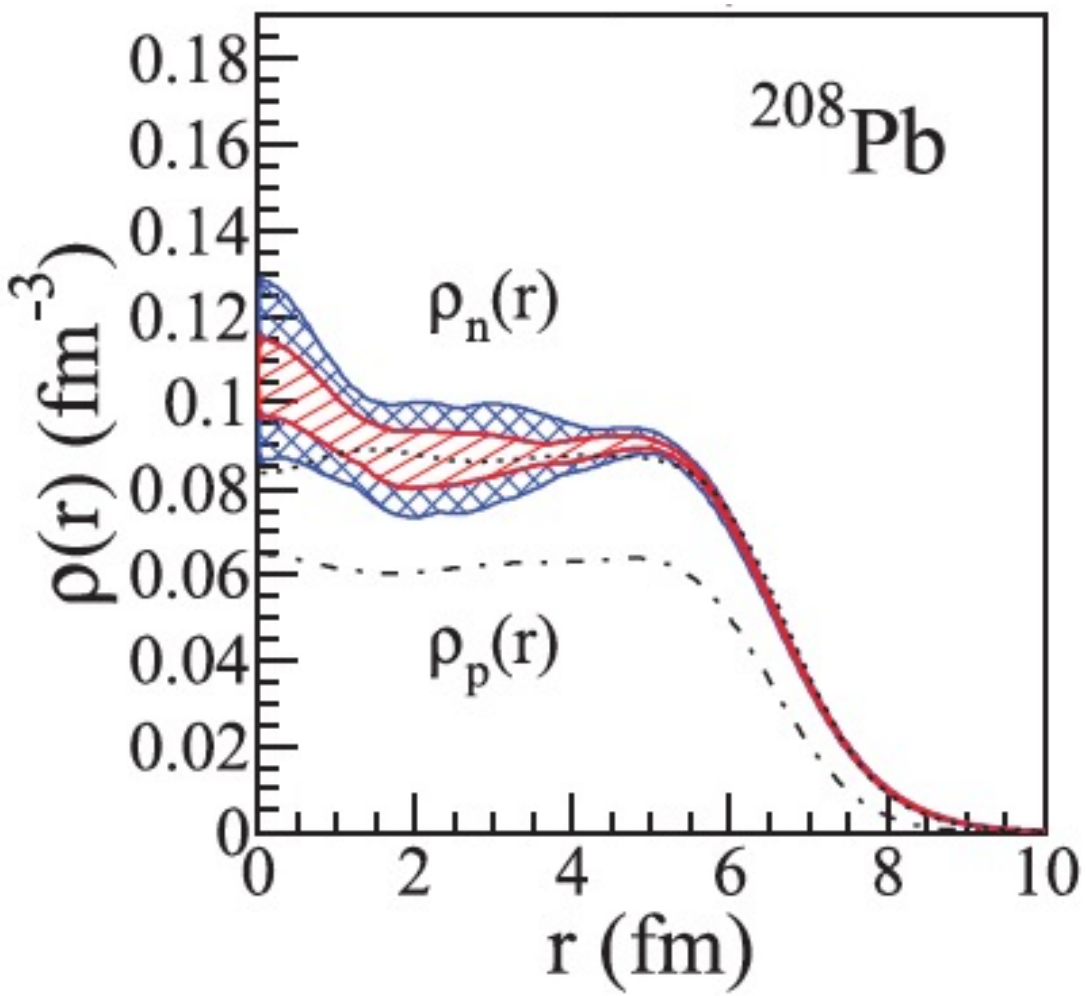

J. Zenihiro, *et al.*, Phys. Rev. C **82**, 44611 (2010).

J. Zenihiro et al., polarized proton elastic experiments

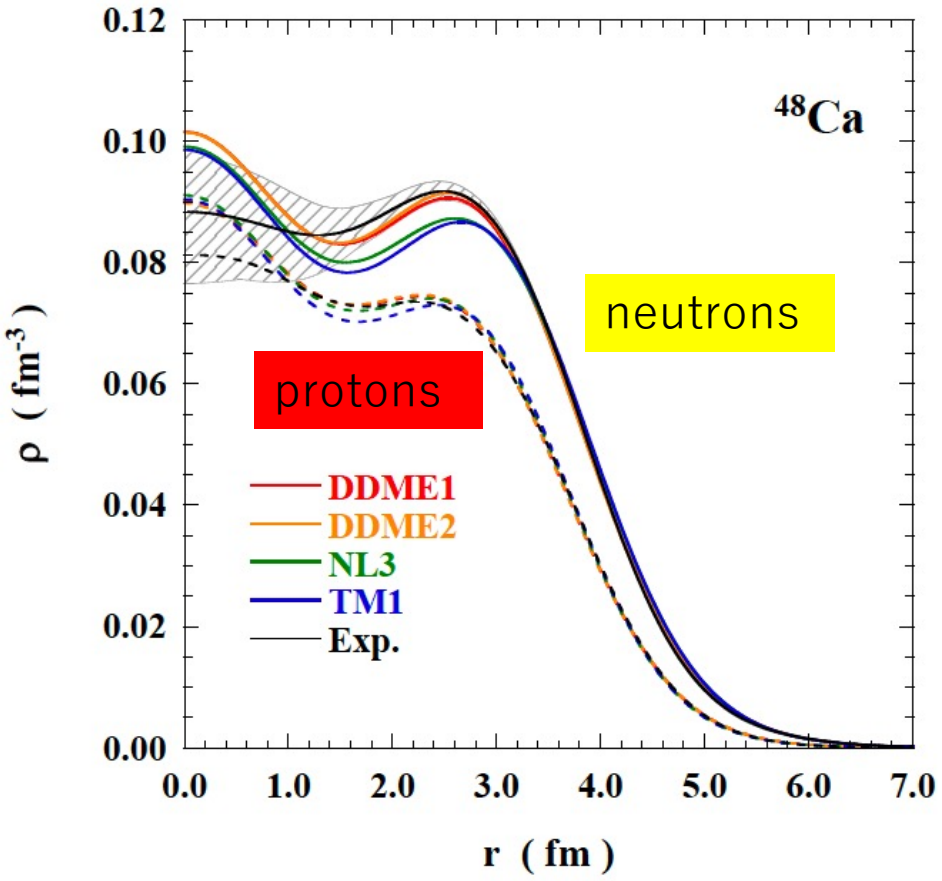

FIG. 1. (color on line) Proton and neutron densities of ^{48}Ca with RMF interactions DDME1, DDME2, NL3 and TM1. Neutron (proton) densities are plotted by solid (dashed) lines. The black solid line shows experimental data taken ref. [32]. The shaded area of experimental data show experimental uncertainties of statistical and systematic errors.

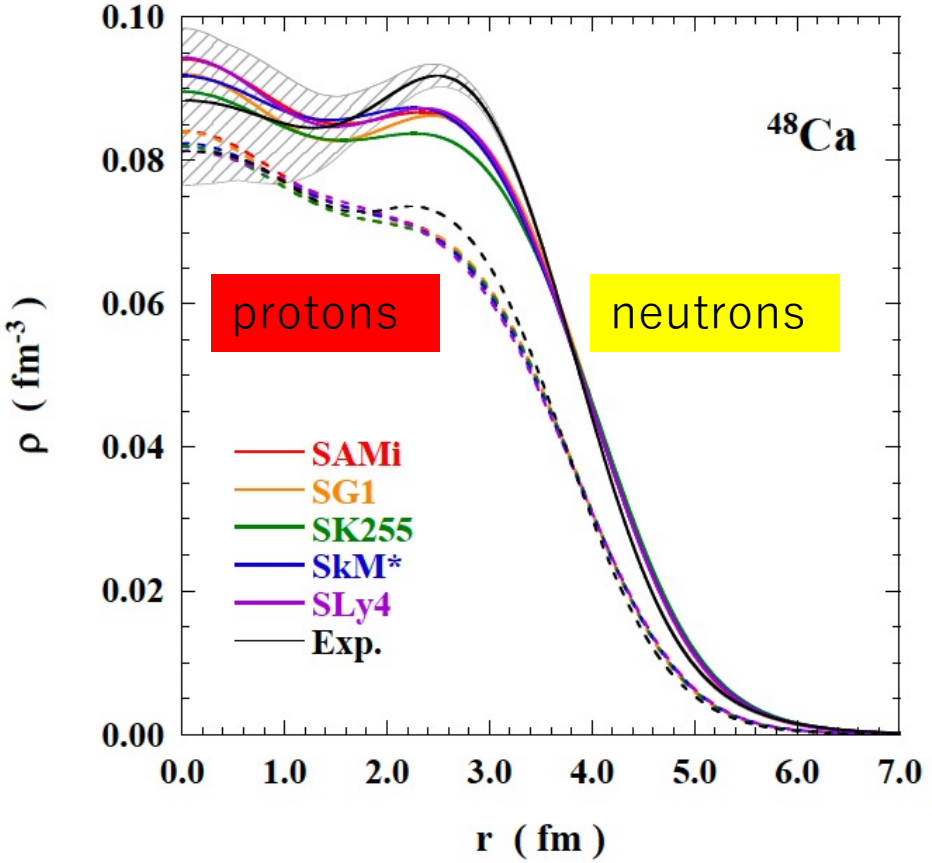

FIG. 2. (color on line) The same as Fig. 1, but with Skyrme interactions SAMi, SG1, SK255, SkM* and SLy4..

The shaded are is the experimental statistical and systematic errors.

Proton elastic scattering
J. Zenihiro et al.,

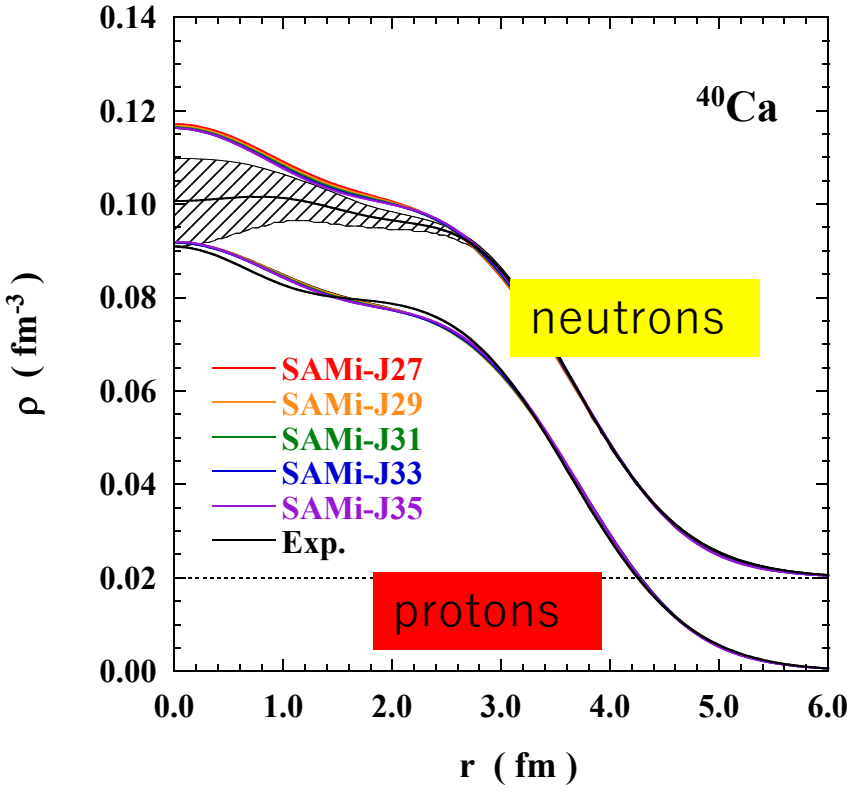

Protons: electron scatterings

Modified neutron density

Empirical occupation probabilities of ^{40}Ca

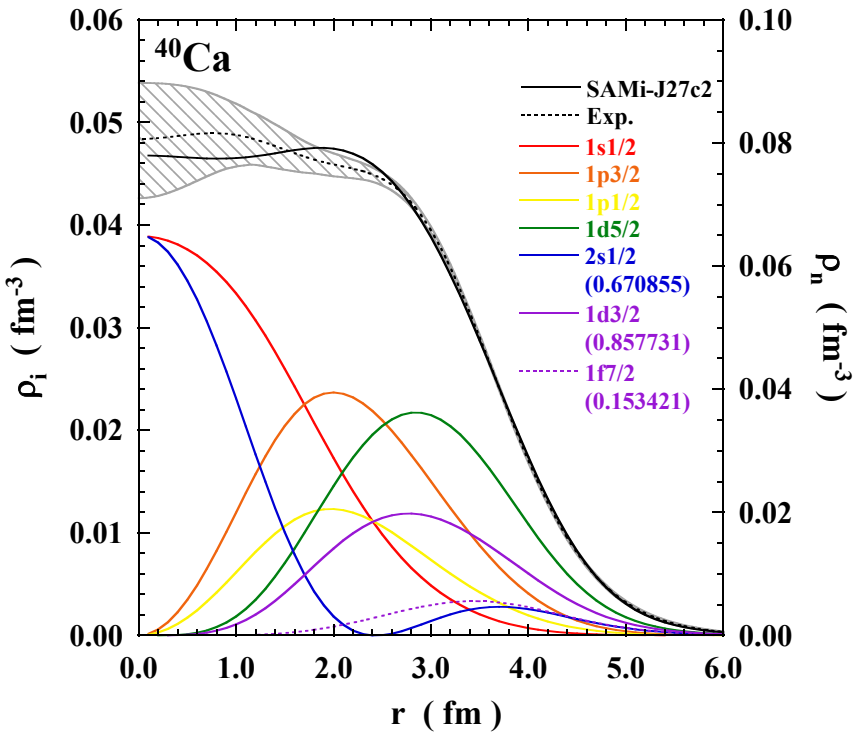

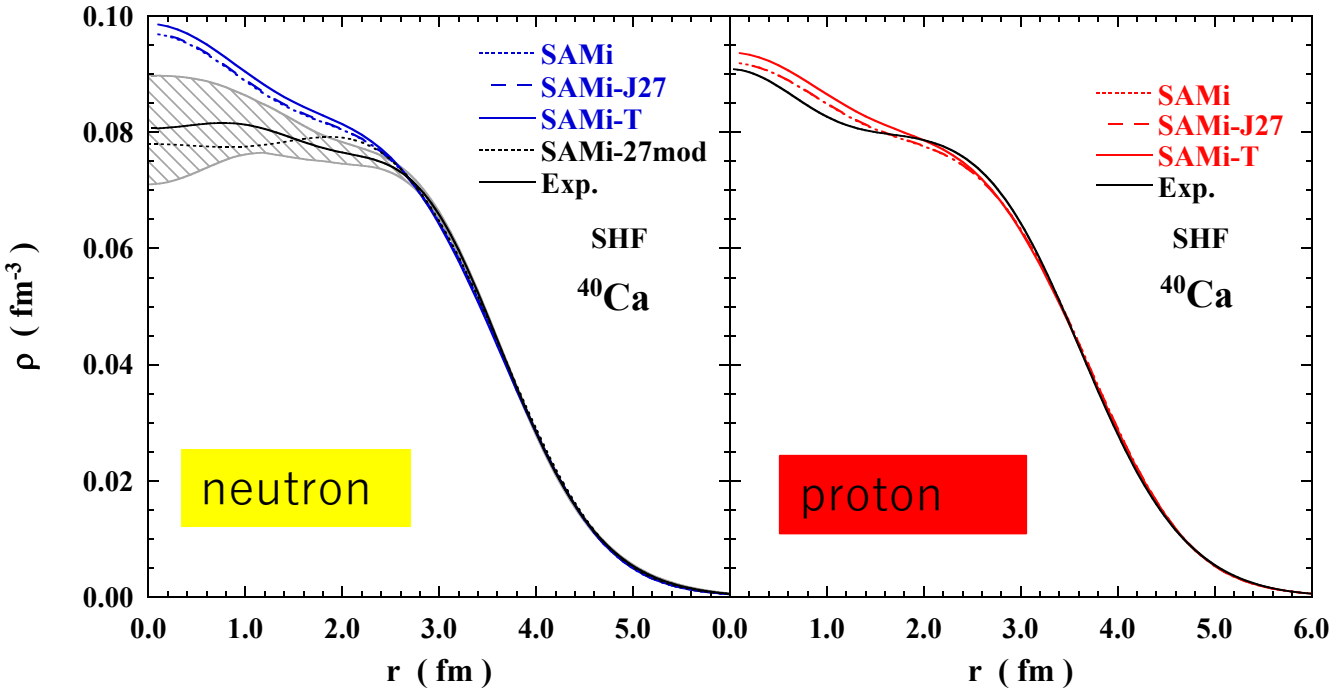

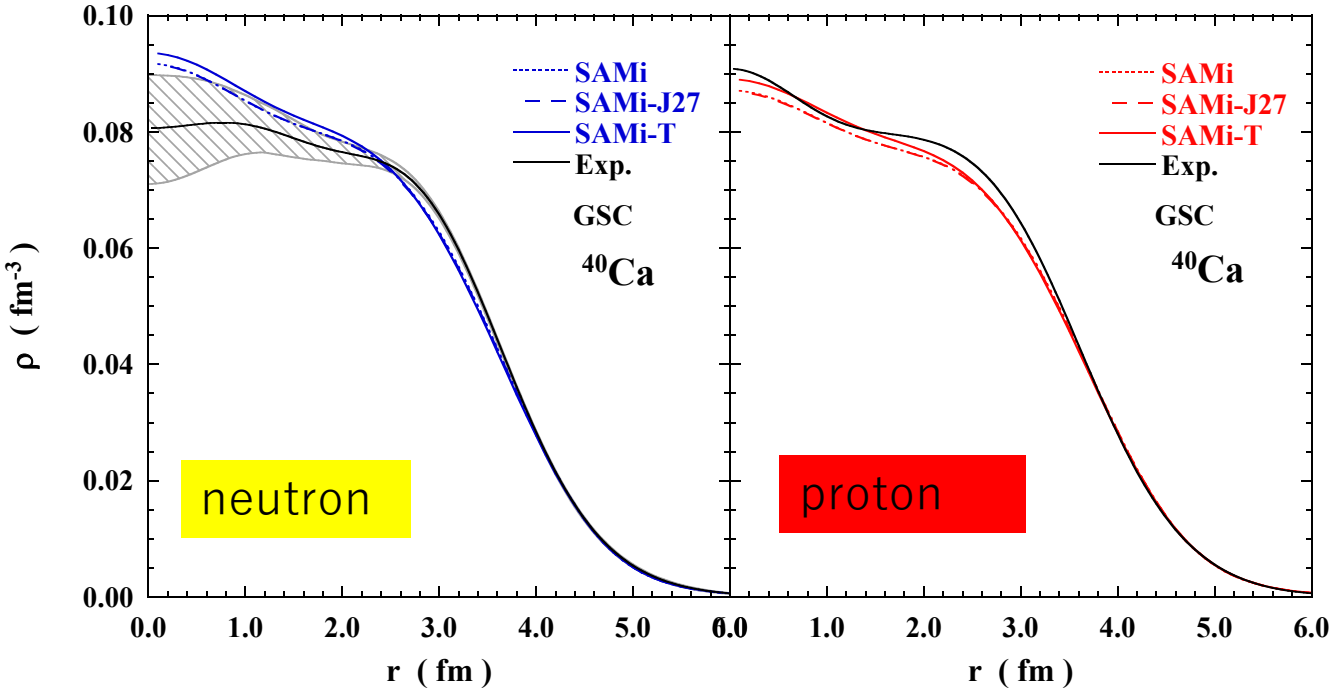

Self-consistent HF+RPA phonon ground state correlations
F. Minato et al,, to be published (2022)

$$\rho_q(r) = \sum_{k=m,i} n_k \frac{2j_k+1}{4\pi} |\varphi_k(r)|^2 \quad (q = p, n), \tag{1}$$

where φ_k and j_k are the single-particle wave function of radial part and total angular momentum for state k, respectively. Here, we used m for particle states and i for hole states. The occupation probabilities are $n_m = 0$ and $n_i = 1$ for the unperturbed density distribution. In case of the perturbed density distributions, they are modified within the number-operator method [4] to

$$n_m = \frac{1}{2(2j_m+1)} \sum_{i\lambda J\pi} (2J+1) |Y_{mi}(\lambda J^\pi)|^2$$
$$n_i = 1 - \frac{1}{2(2j_i+1)} \sum_{m\lambda J\pi} (2J+1) |Y_{mi}(\lambda J^\pi)|^2 . \tag{2}$$

where $Y_{mi}(\lambda J^\pi)$ is the backward amplitude of the phonon operator of random phase approximation. The label λ and J^π represent an RPA phonon state and its spin-parity state, respectively.

^{40}Ca is a good core?
Ground state correlations (GSC)

Table 2: Particle occupation numbers, $(2j+1)v_j^2$, in *sd*-shell to *pf* shell configurations in ^{40}Ca. The column with a bar (—) is not involved in the shell model calculations. Experimental data of proton transfer reaction are taken from Ref. [9].

Model	$2s_{1/2}$	$2p_{3/2}$	$2p_{1/2}$	$1d_{5/2}$	$2s_{1/2}$	$1d_{3/2}$	$1f_{7/2}$	$2p_{3/2}$	$2p_{1/2}$	$1f_{5/2}$
HFB (SAMi)	2.00	4.00	2.00	6.00	2.00	4.00	0.00	0.00	0.00	0.00
HF+GSC(SAMi:π)	1.964	3.908	1.949	5.761	1.843	3.792	0.206	0.049	0.010	0.040
HF+GSC(SAMi-T:π)	1.968	3.905	1.954	5.753	1.845	3.776	0.201	0.052	0.009	0.076
GSC (RPA) [6]	1.92	3.76	1.88	5.58	1.8	3.7	0.24	0.16	0.08	—
dpf-shell [7]	—	—	—	—	—	3.30	0.63	0.07	—	—
sdpf-msd4 [8]	—	—	—	5.902	1.908	3.477	0.617	0.096	—	—
sdpf-mu (2*p*-2*h*)	—	—	—	5.864	1.933	3.845	0.191	0.040	0.020	0.107
sdpf-mu (4*p*-4*h*)	—	—	—	5.727	1.854	3.660	0.421	0.089	0.041	0.208
exp. (p-transfer) [9]	—	—	—	6.0	1.70	3.59	0.56	0.15		
exp. (neutron density) [10]	2.00	4.00	2.00	6.00	1.342	3.431	1.227			

HF+GSC, F. Minato et al., to be published (2022)

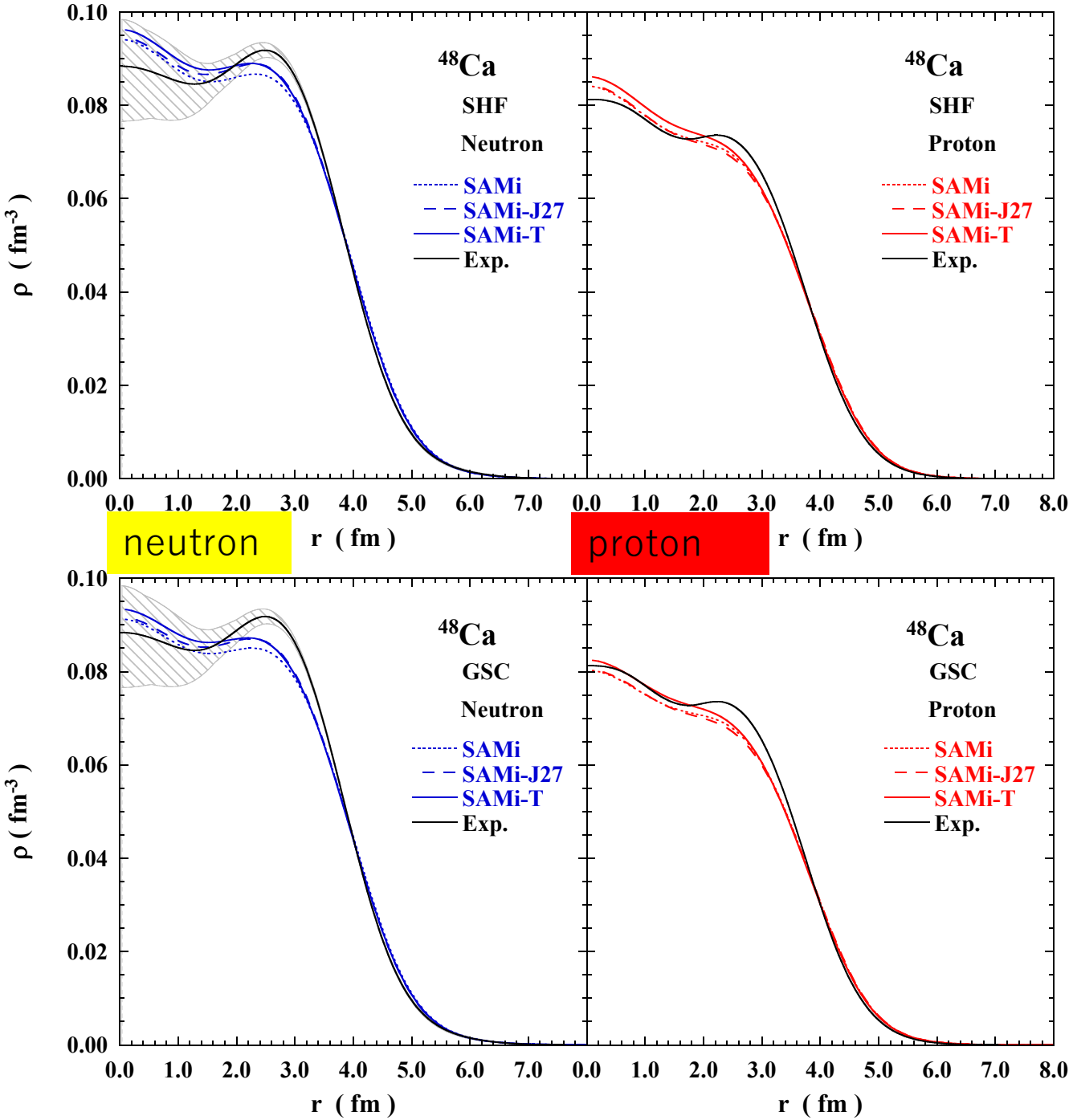
48Ca
SHF
Neutron
SAMi
SAMi-J27
SAMi-T
Exp.
48Ca
SHF
Proton
SAMi
SAMi-J27
SAMi-T
Exp.
neutron
proton
48Ca
GSC
Neutron
SAMi
SAMi-J27
SAMi-T
Exp.
48Ca
GSC
Proton
SAMi
SAMi-J27
SAMi-T
Exp.
ρ (fm-3)
r (fm)
0.00
0.02
0.04
0.06
0.08
0.10
0.0
1.0
2.0
3.0
4.0
5.0
6.0
7.0
8.0

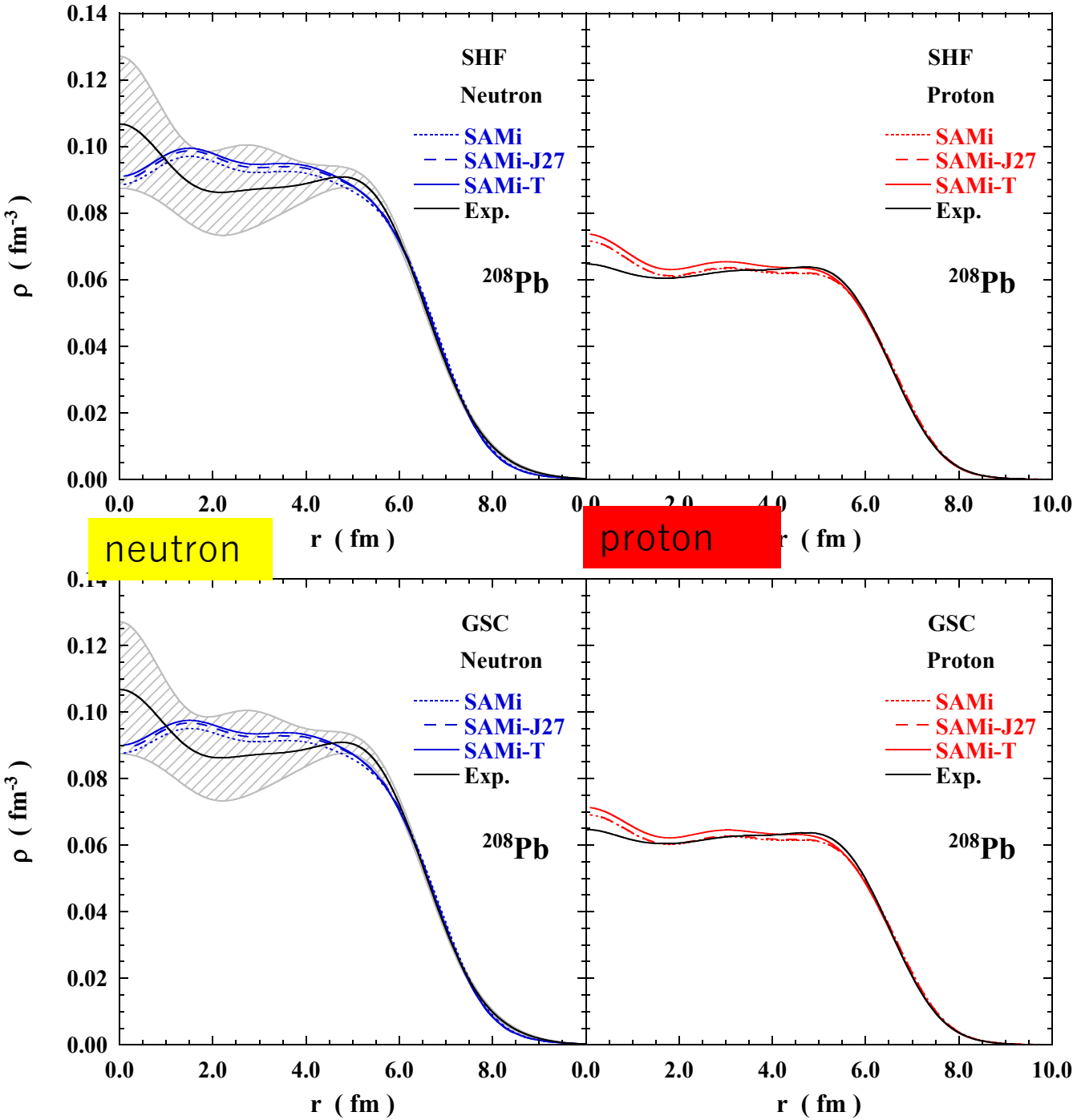
SHF
Neutron
SAMi
SAMi-J27
SAMi-T
Exp.
208Pb
SHF
Proton
SAMi
SAMi-J27
SAMi-T
Exp.
208Pb
ρ (fm-3)
r (fm)
neutron
proton
GSC
Neutron
SAMi
SAMi-J27
SAMi-T
Exp.
208Pb
GSC
Proton
SAMi
SAMi-J27
SAMi-T
Exp.
208Pb
ρ (fm-3)
r (fm)
r (fm)

Table 1: Proton and neutron radii of ^{40,48}Ca and ^{208}Pb. The neutron skin is given as Δr_{np}. HF denotes the results of HF calculations, while HF+GSC includes also the ground state correlations. The experimental data are taken from Zenihiro et al. The radii are given in unit of fm.

		SAMi		SAMi-27		SAMi-T		
Nuclei		HF	HF+GSC	HF	HF+GSC	HF	HF+GSC	exp.
^{40}Ca	n	3.343	3.773	3.344	3.810	3.339	3.808	3.375
	p	3.390	3.853	3.391	3.870	3.386	3.845	3.385
	Δr_{np}	−0.047	−0.080	−0.047	−0.060	−0.046	−0.037	−0.010
^{48}Ca	n	3.612	4.003	3.588	4.006	3.589	4.004	3.555
	p	3.436	3.770	3.444	3.801	3.424	3.781	3.387
	Δr_{np}	0.176	0.233	0.144	0.205	0.166	0.223	0.168
^{208}Pb	n	5.610	5.750	5.580	5.731	5.574	5.730	5.653
	p	5.463	5.555	5.456	5.553	5.421	5.517	5.442
	Δr_{np}	0.147	0.195	0.123	0.178	0.153	0.213	0.211

The Nuclear Equation of State: Infinite System

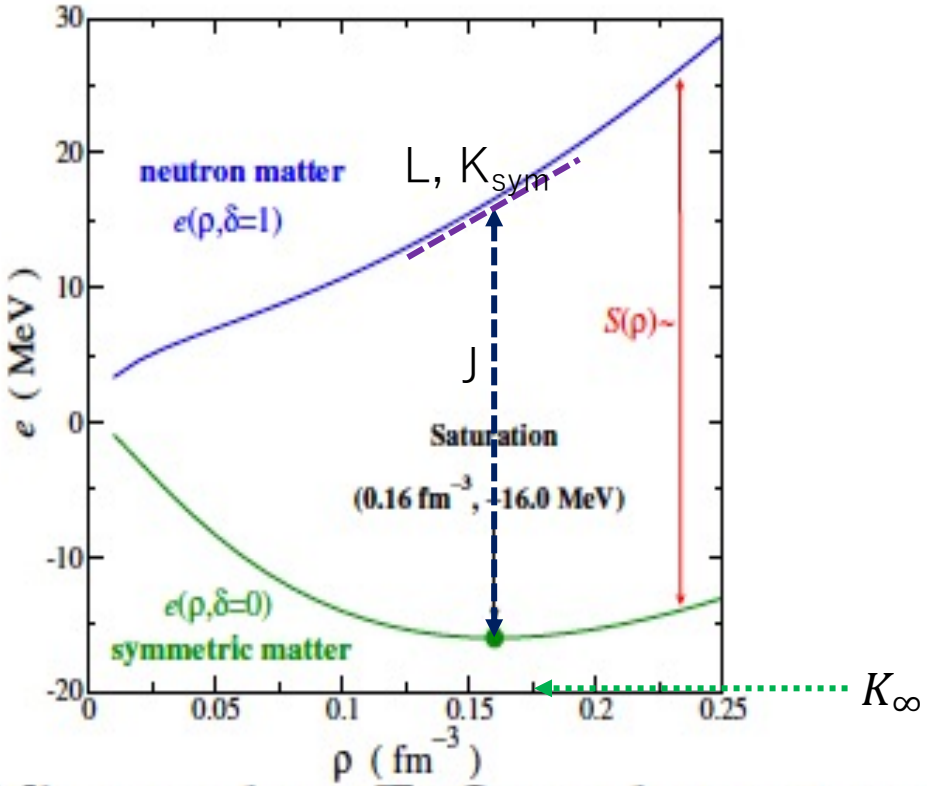

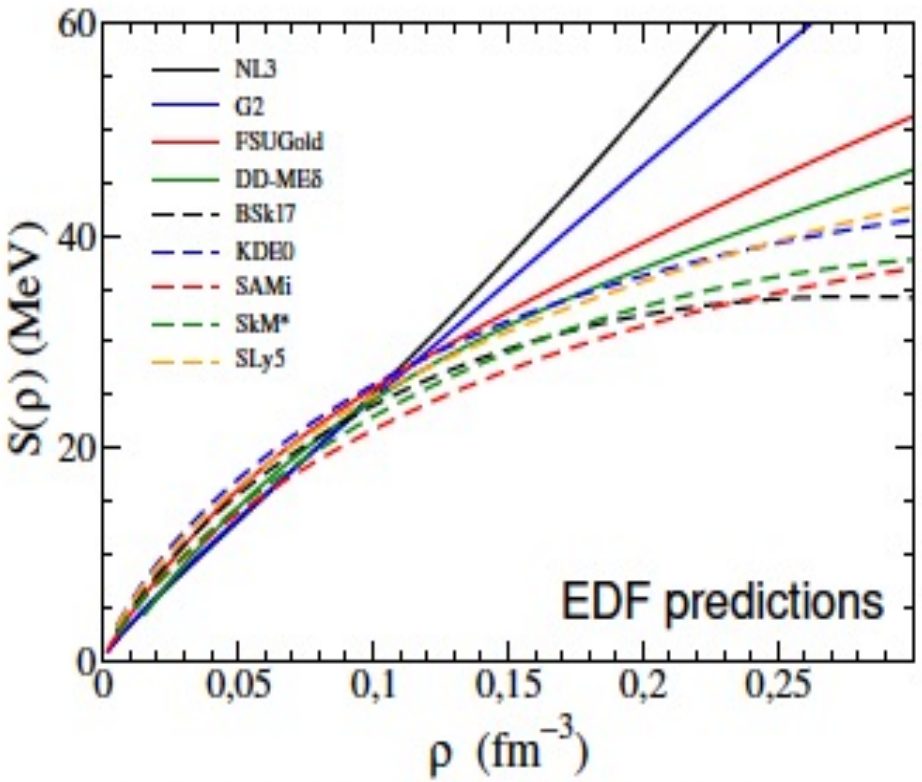

* The nuclear EoS can be written in good approximation as:

$$e(\rho,\beta) \approx e(\rho,\beta=0) + S(\rho)\beta^2 \text{ where } \beta \equiv \frac{\rho_n - \rho_p}{\rho_n + \rho_p}$$

$$S(\rho) = J(\rho_0) + L(\rho_0)\frac{\rho-\rho_0}{3\rho_0} + K_{sym}(\rho_0)\frac{1}{2}\left(\frac{\rho-\rho_0}{3\rho_0}\right)^2 + \cdots$$

Examples: EoS parameters from nuclear observables

Isovector properties (e.g. $S(\rho)$) are thought to be well determined by the **neutron skin thickness** ($\Delta r_{np} \equiv \langle r_n^2 \rangle^{1/2} - \langle r_p^2 \rangle^{1/2}$) **of a heavy nucleus such as ^{208}Pb)**:

Macroscopic model: $\Delta r_{np} \sim \frac{1}{12} \frac{(N-Z)}{A} \frac{R}{J} L \quad (L \propto p_0^{neut})$

^{208}Pb

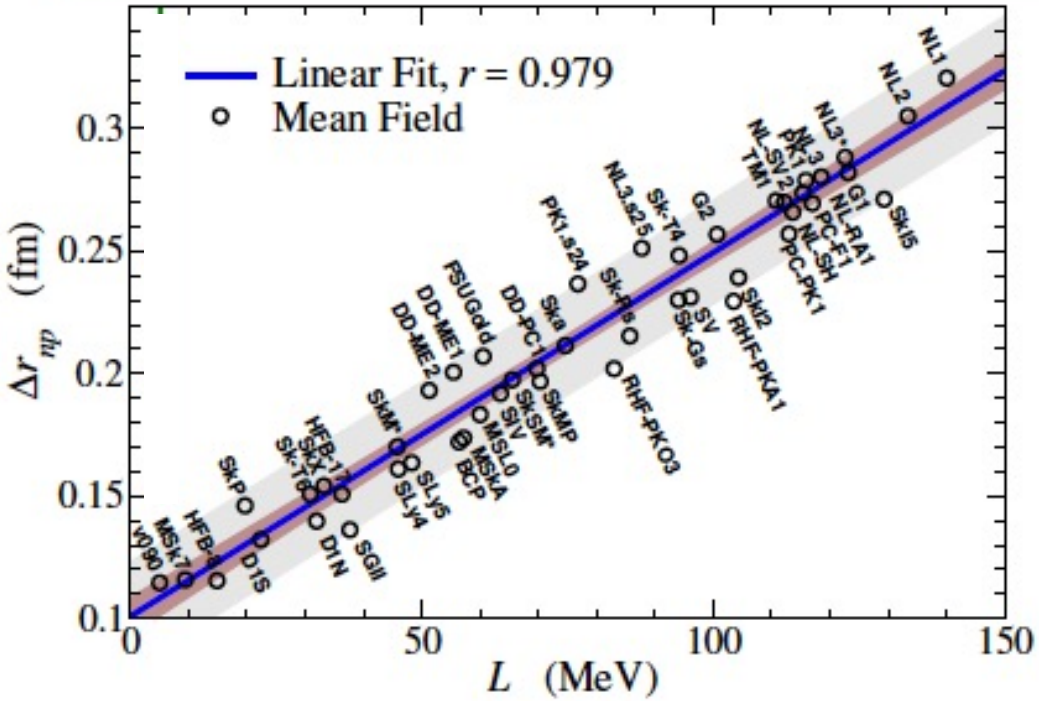

X. Roca-Maza

Physical Review Letters **106**, 252501 (2011)

Micorscopic models (EDFs) confirm such a relation

However the experimental precision and accuracy needed in the measurment of this property is very challenging nowadays.

EDF incompressibility and symmetry energy J, L, K

The equation of state (EoS) of symmetric nuclear matter (SNM), the first term of Eq. (3), can be expanded as

$$\varepsilon(\rho, I = 0) \approx \varepsilon(\rho_0, I = 0) + \frac{1}{9} K_\infty \delta^2 + \cdots , \qquad (9)$$

where $\delta = \frac{\rho - \rho_0}{\rho_0}$ and the incompressibility $K\infty$ in SNM is defined by

$$K_\infty = 9\rho^2 \frac{\partial^2}{\partial \rho^2} (\varepsilon(\rho, I = 0))\Big|_{\rho=\rho_0} . \qquad (10)$$

The SNM incompressibility is often related with the incompressibility of finite nuclei, extracted from the IS giant monopole resonance as

$$K_A = K_\infty + K_{\text{surf}} A^{-1/3} + K_\tau I^2 + K_{\text{Coul}} \frac{Z^2}{A^{4/3}}, \qquad (11)$$

$$K_\tau = K_{sym} + 3L - LB$$

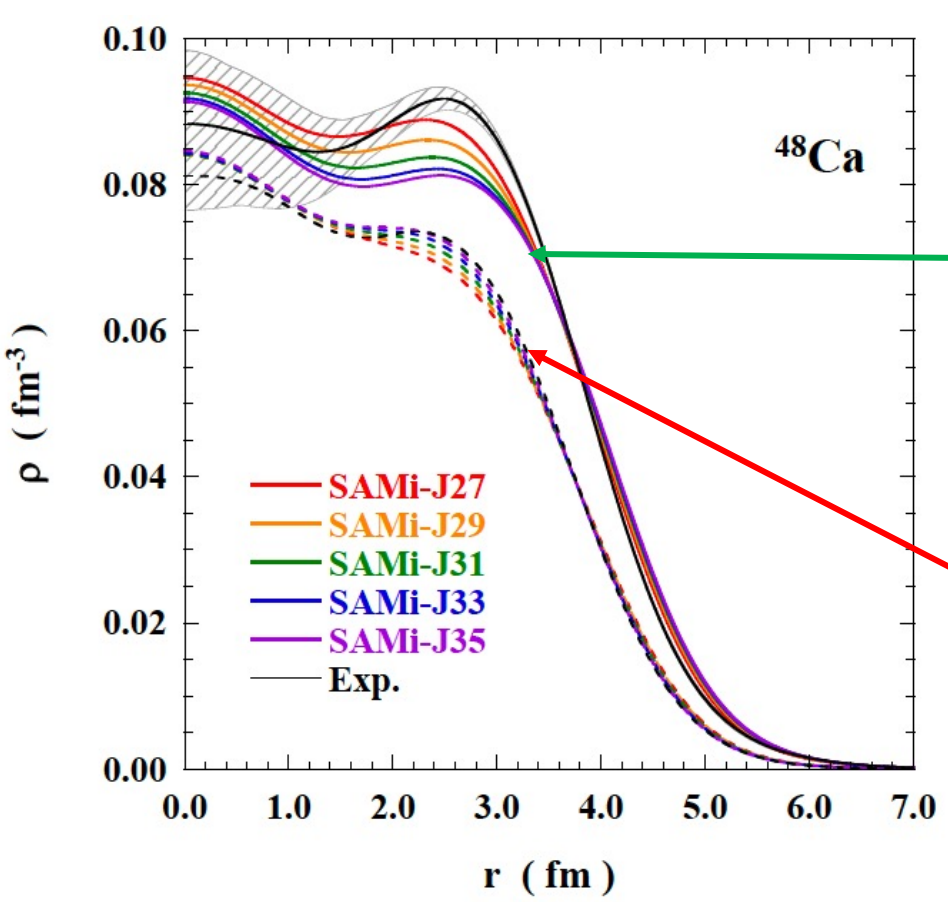

neutrons

protons

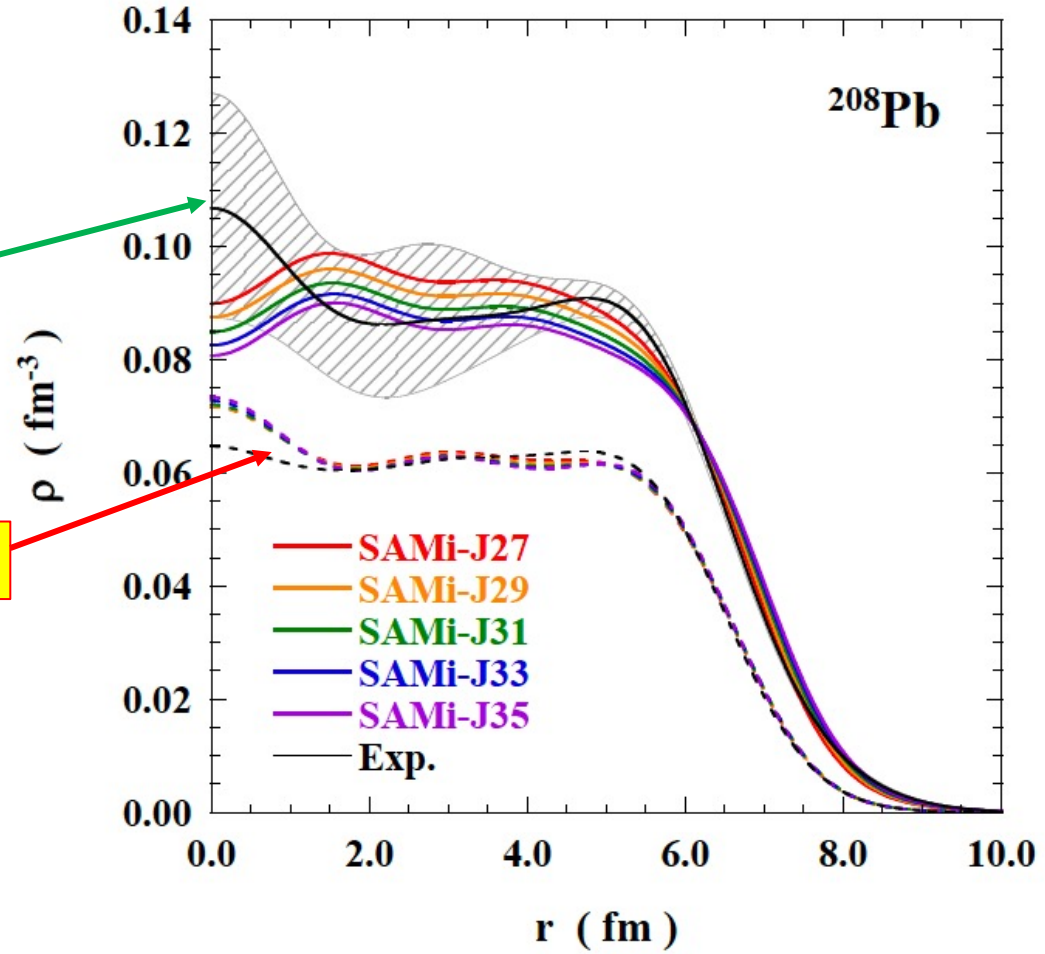

FIG. 4. (color on line) The same as Fig. 1, but with SAMi-J interactions.

FIG. 8. (color on line) The same as Fig. 5, but with SAMi-J interactions.

Larger J gives large neutron skin.

2D plot of IS and IV densities

$$\rho_{IS}(r) = \rho_n(r) + \rho_p(r),$$
$$\rho_{IV}(r) = \rho_n(r) - \rho_p(r).$$

S. Yoshida et al., Phys. Rev. C102, 064307/pp. 1-12 (2020)

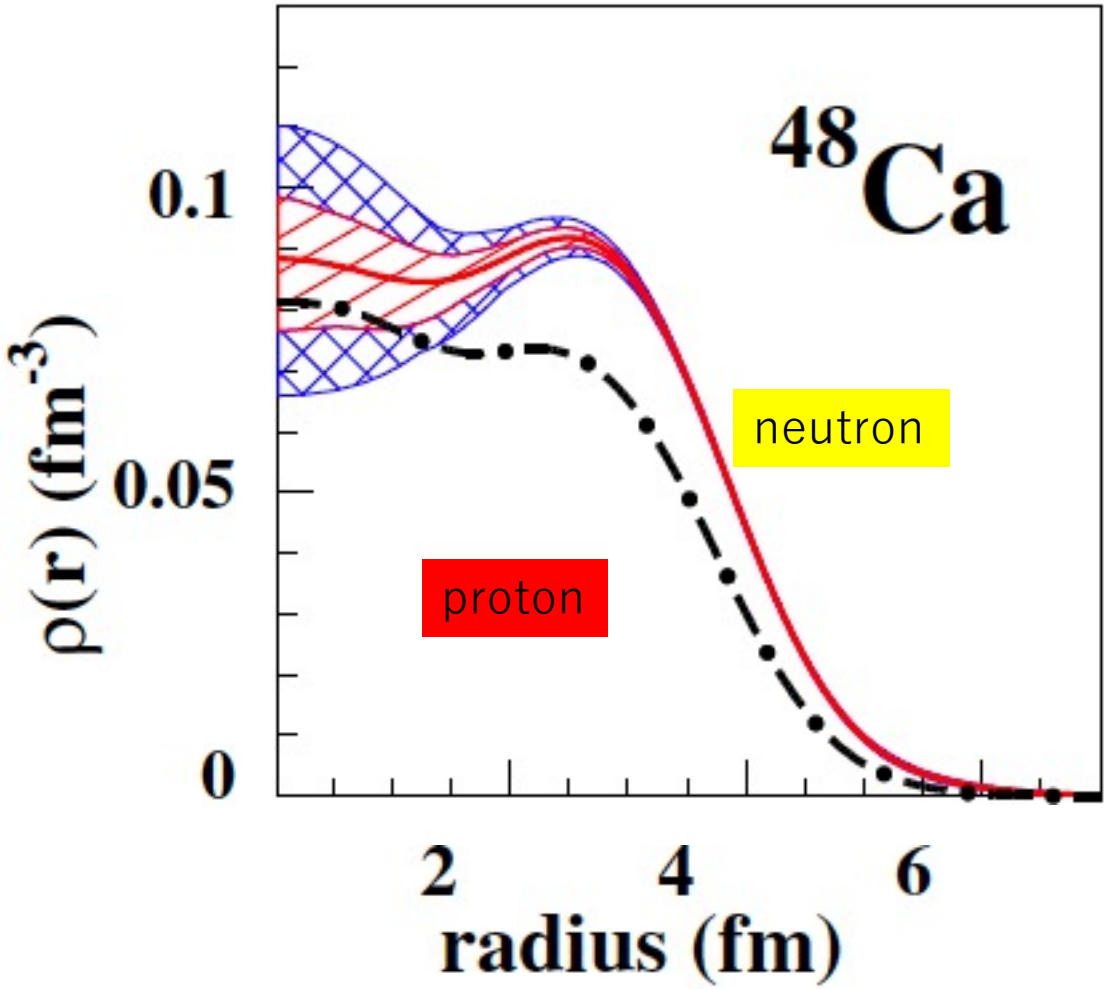

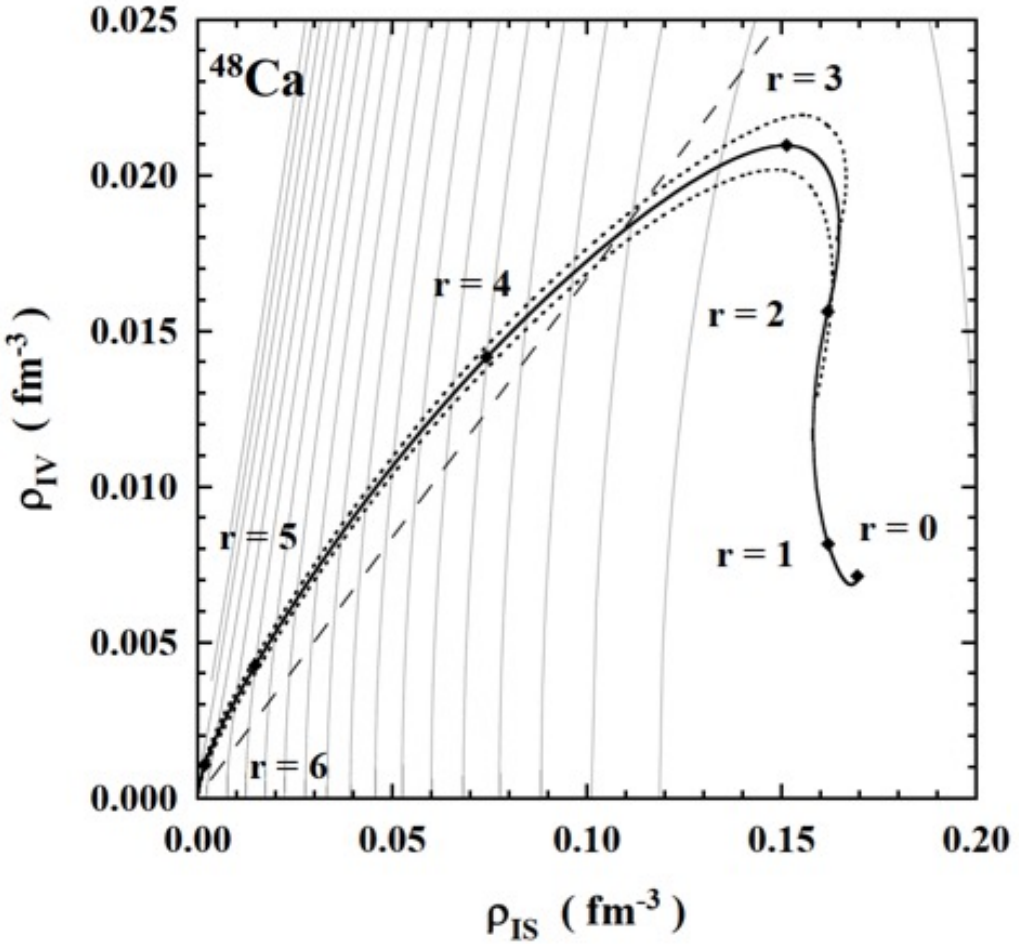

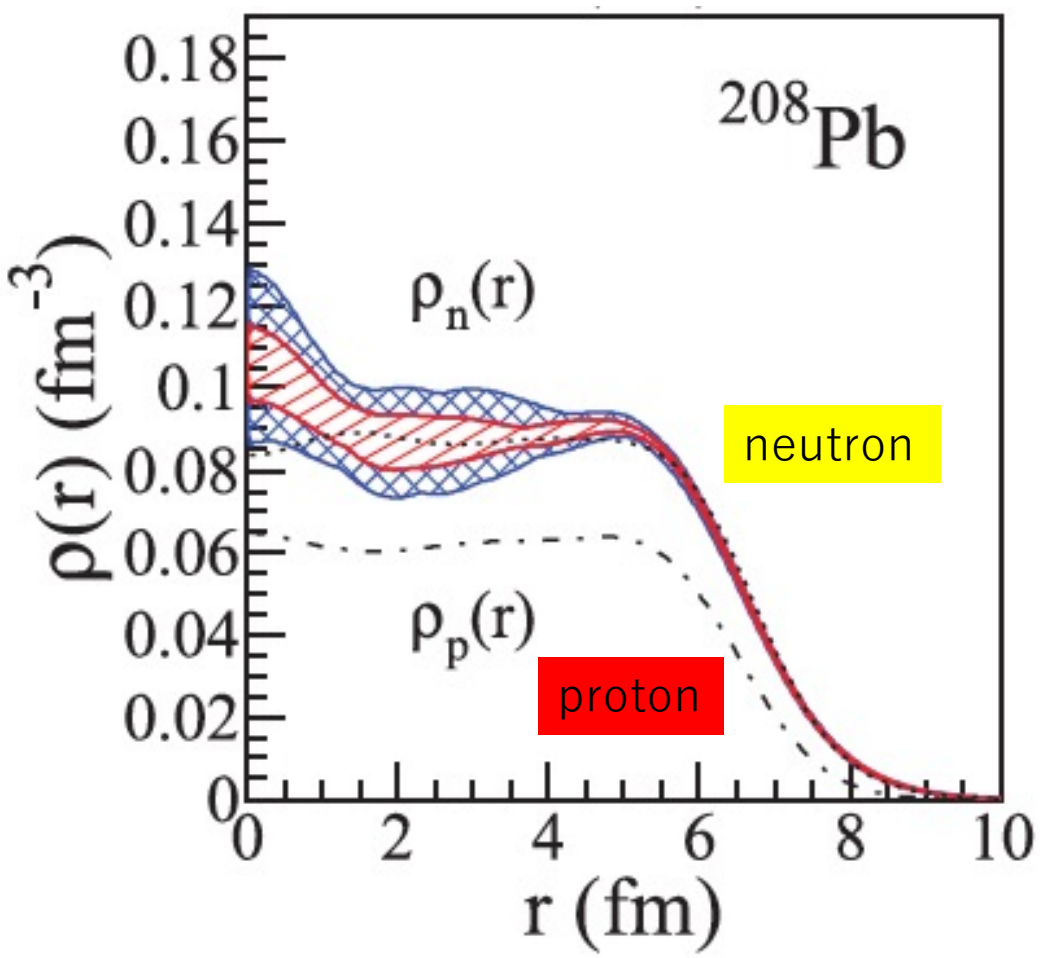
^{208}Pb
$\rho_n(r)$
$\rho_p(r)$
neutron
proton
$\rho(r)$ (fm^{-3})
r (fm)
0.18
0.16
0.14
0.12
0.1
0.08
0.06
0.04
0.02
0
0
2
4
6
8
10

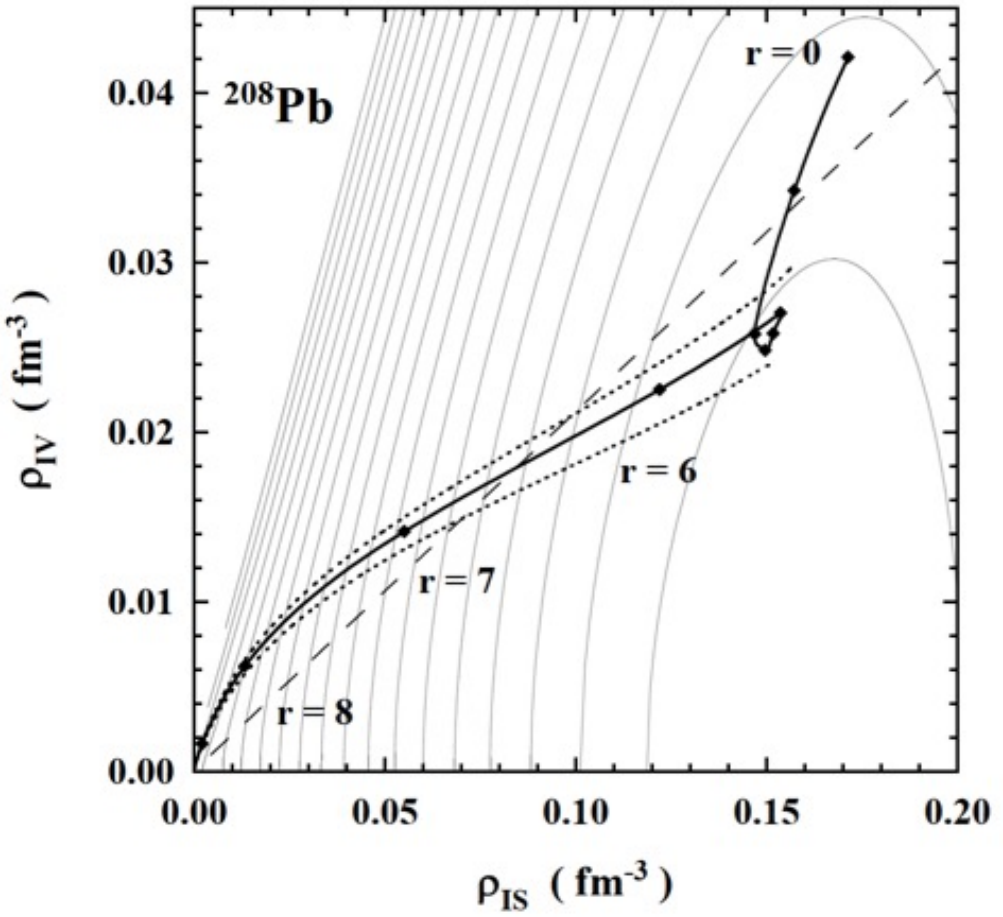
^{208}Pb
r = 0
r = 6
r = 7
r = 8
ρ_{IV} (fm^{-3})
ρ_{IS} (fm^{-3})
0.04
0.03
0.02
0.01
0.00
0.00
0.05
0.10
0.15
0.20

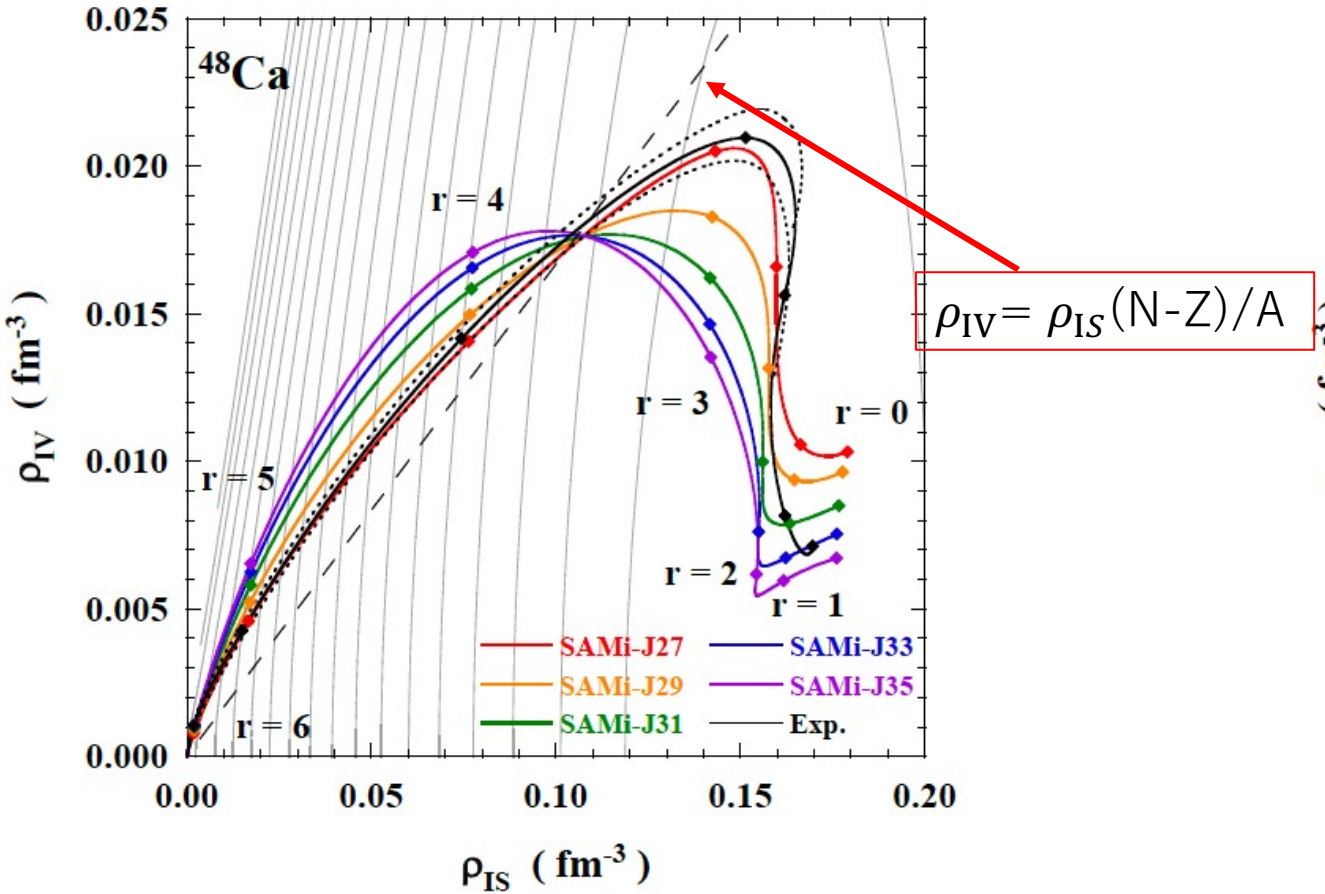

$\rho_{IV} = \rho_{IS}(N-Z)/A$

FIG. 9. (color on line) Trajectory in 2D-plot of experimental isoscalar (IS) and isovector (IV) densities of ^{48}Ca. The equi-energy contour lines of HF EDF are calculated by using SAMi-J27 and plotted for the values from 3 MeV at $\rho_{IS} = \rho_{IV} \approx 0$ to -15 or -16 MeV at around the saturation density $\rho_{IS} \approx 0.16$ fm^{-3} with the energy step of 1 MeV. The experimental trajectory is given by a solid curve sandwiched between two dotted lines. The area between two dotted lines shows the experimental uncertainty. The dashed line corresponds to the constant IV density limit $\rho_{IV} = \rho_{IS}(N-Z)/A$. Experimental data is taken ref. [32].

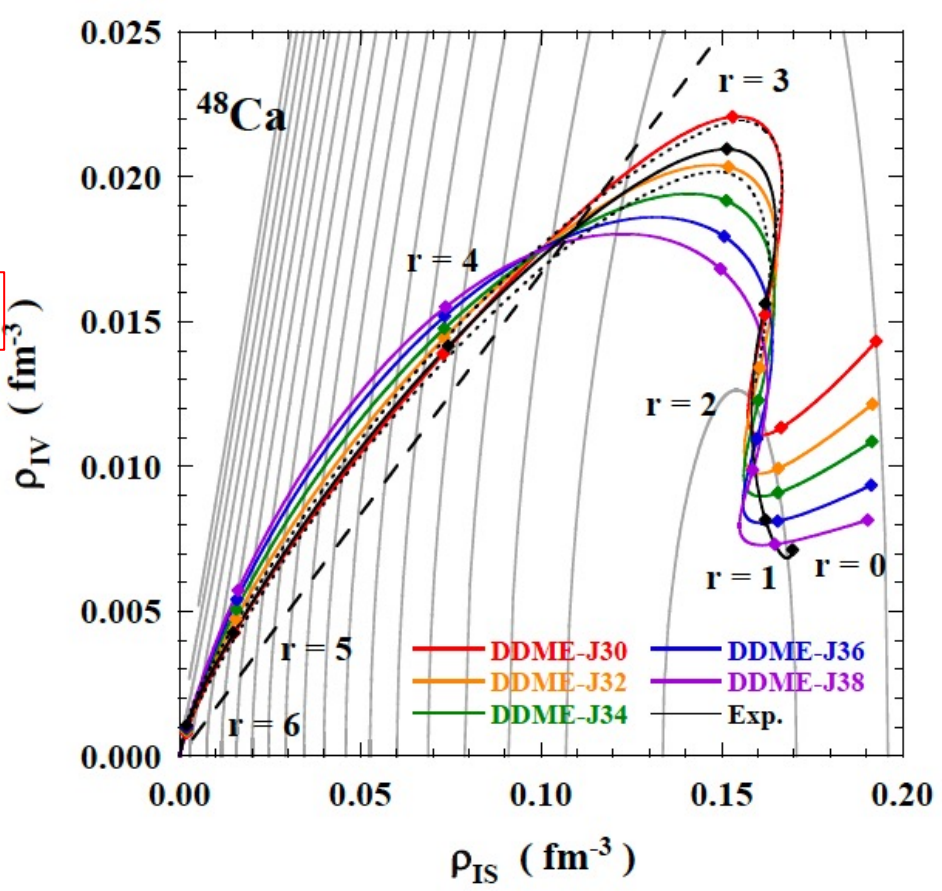

FIG. 13. (color on line) The same as Fig. 11, but with DDME-J interactions. The equi-energy contour lines are plotted for DDME-J30.

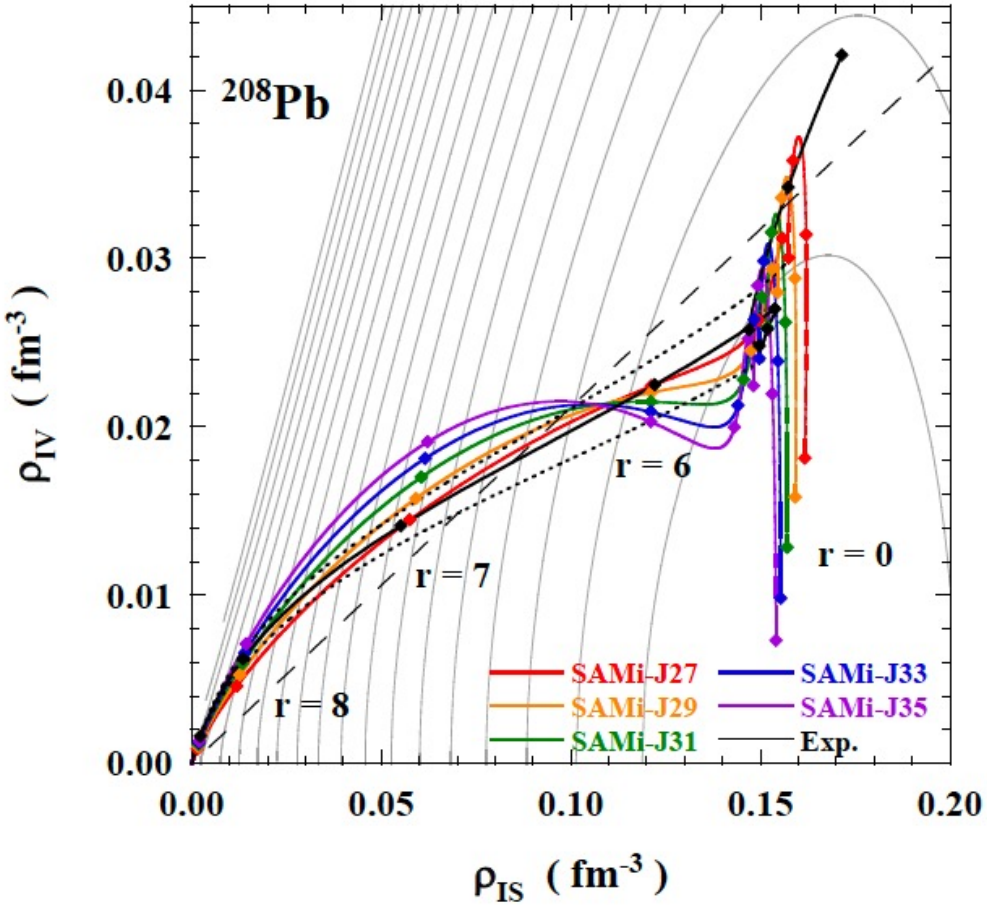

FIG. 18. (color on line) The same as Fig. 15, but with SAMi-J interactions.

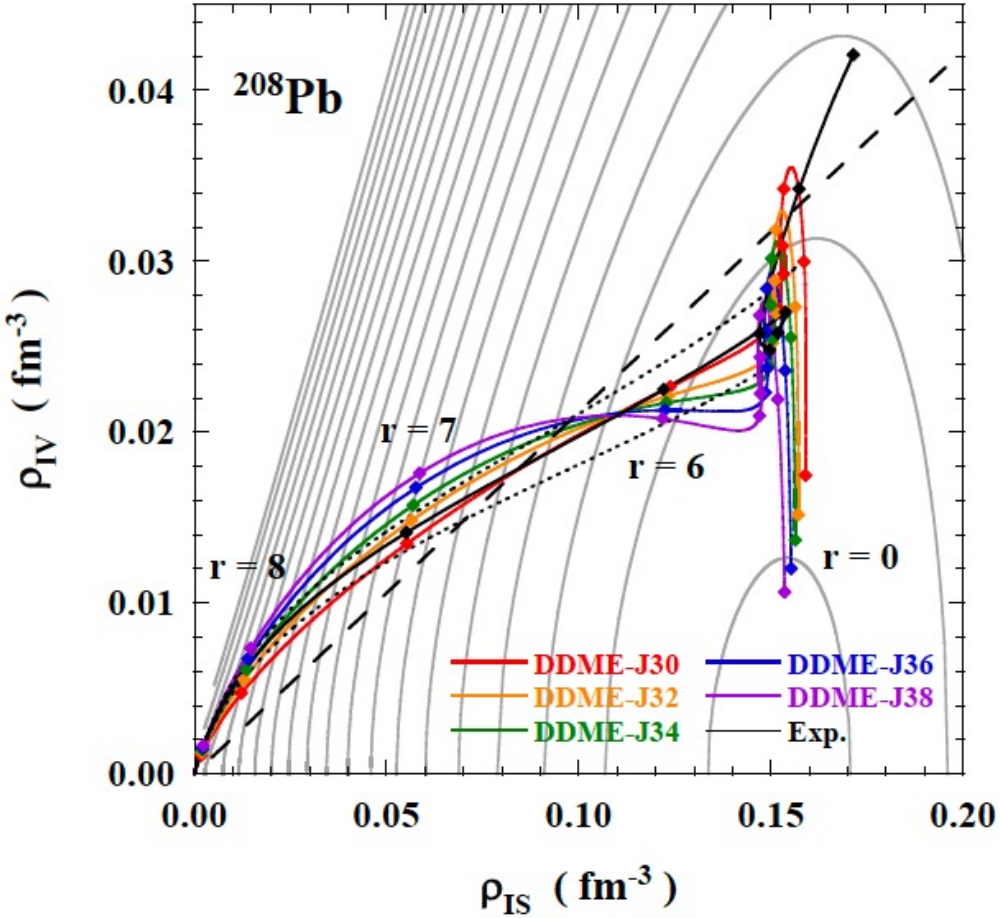

FIG. 17. (color on line) The same as Fig. 15, but with DI interactions.

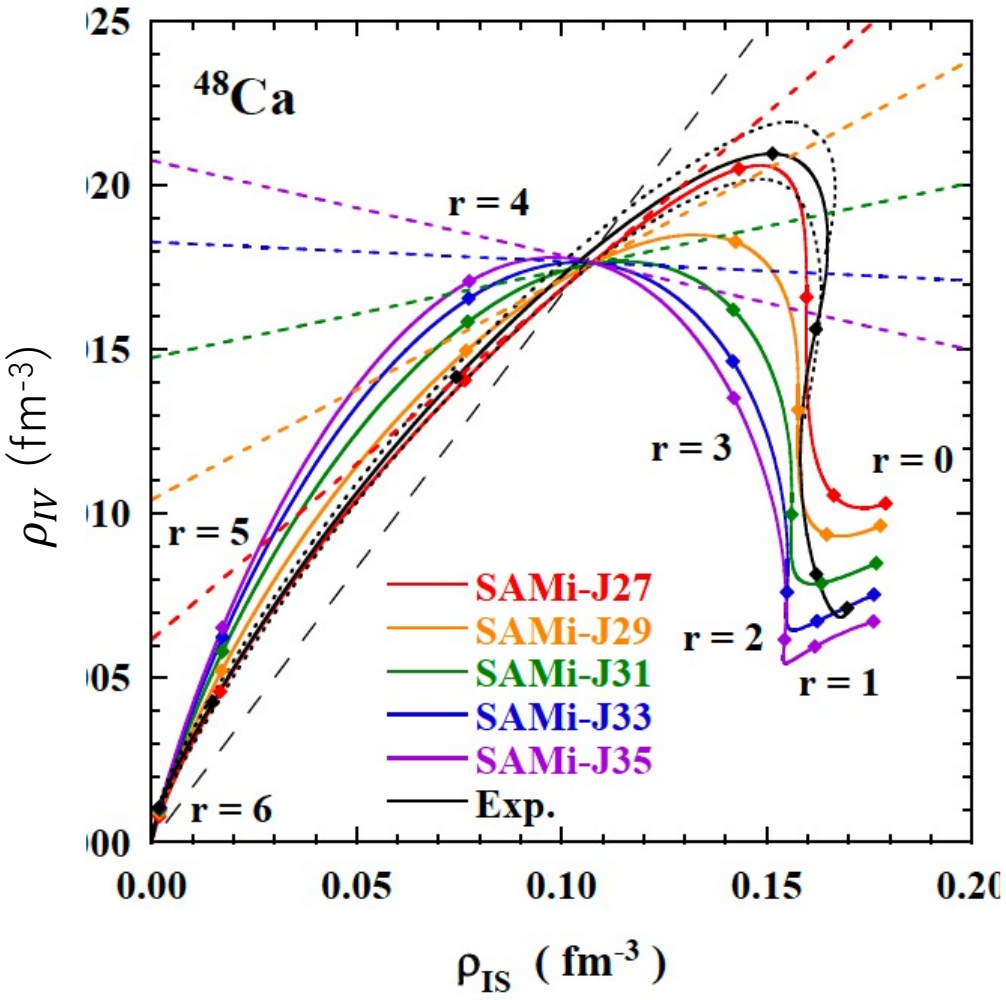

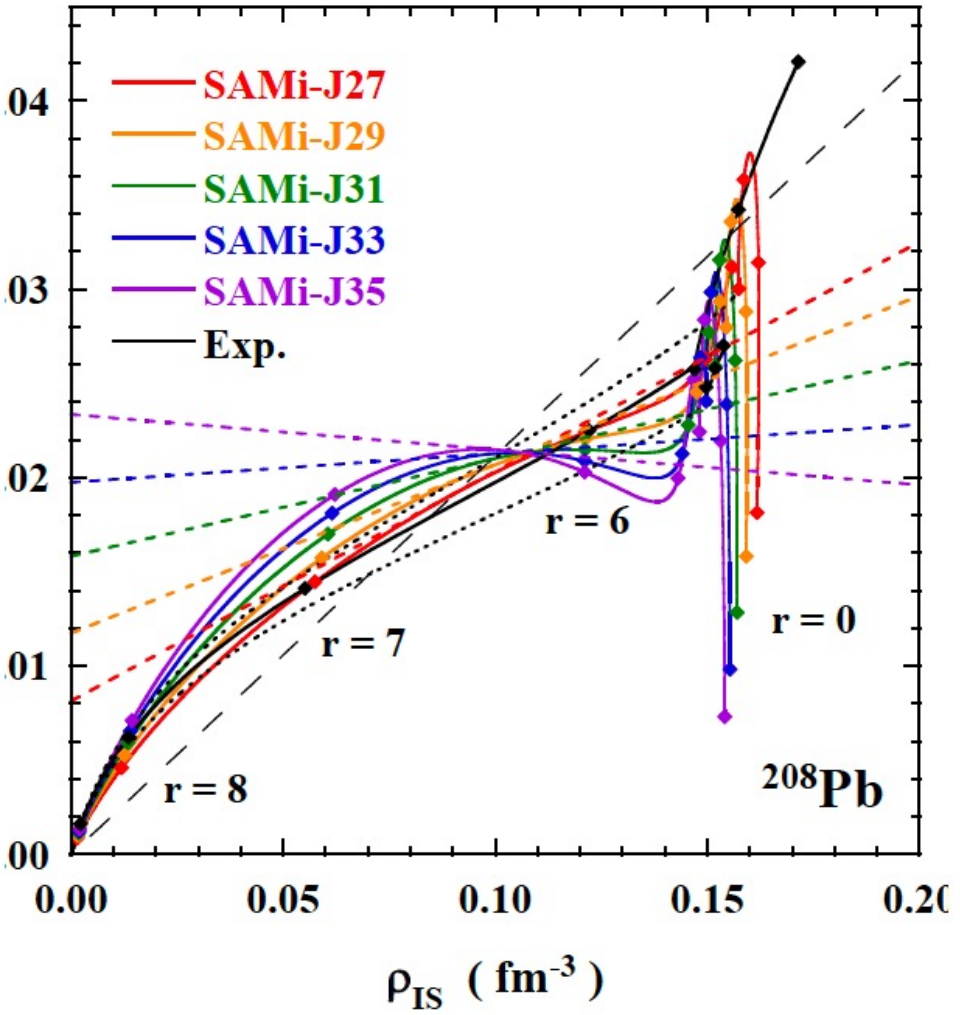

FIG. 19. (color on line) The slope of IS-IV 2D trajectory of ^{48}Ca. The slope is evaluated at the cross point between the IS-IV density trajectory and the constant IV density limit . The SAMi-J family are adopted for the plot.

Symmetry energy coefficients at low density 0.1 fm^{-3}

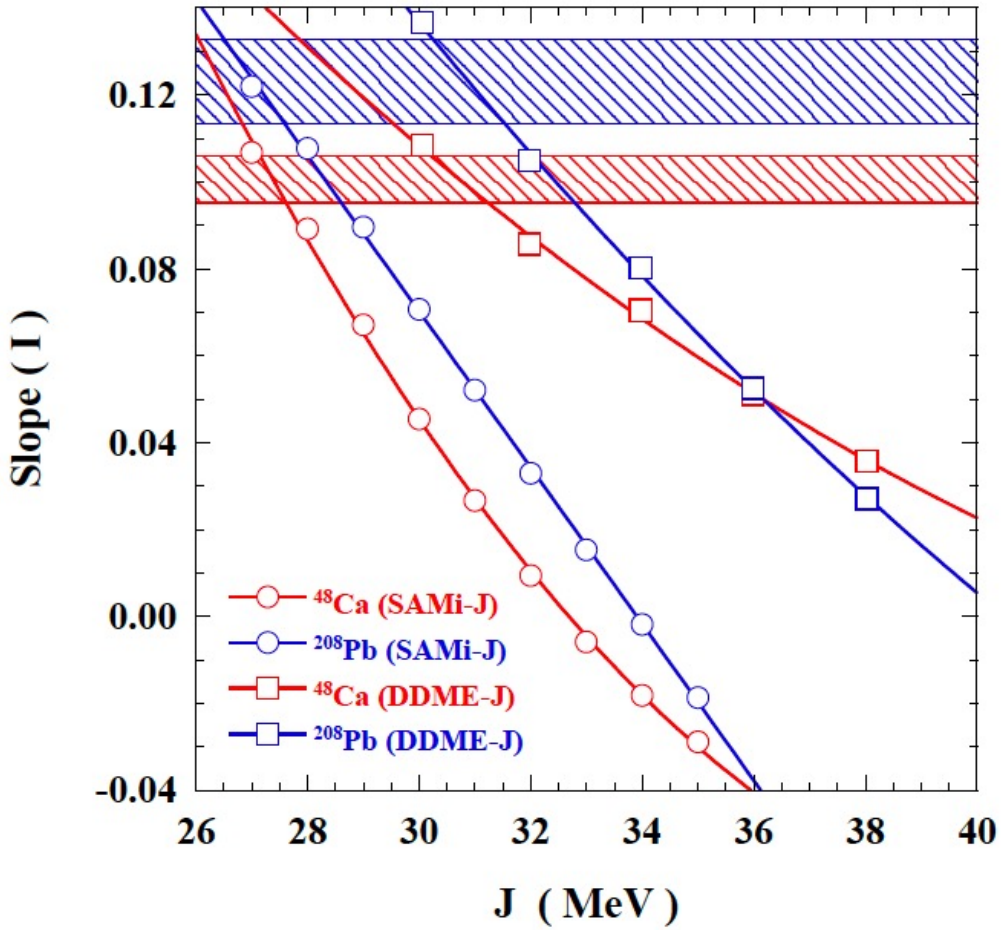

FIG. 21. (color on line) Correlation between the symmetry energy coefficient J and the slope of IS-IV density curve. The SAMI-J and DDME-J families are used for the plots. The shaded areas show experimental slopes obtained of ^{48}Ca and ^{208}Pb, respectively, at the cross point between the IS-IV density trajectory and the constant IV density limit .

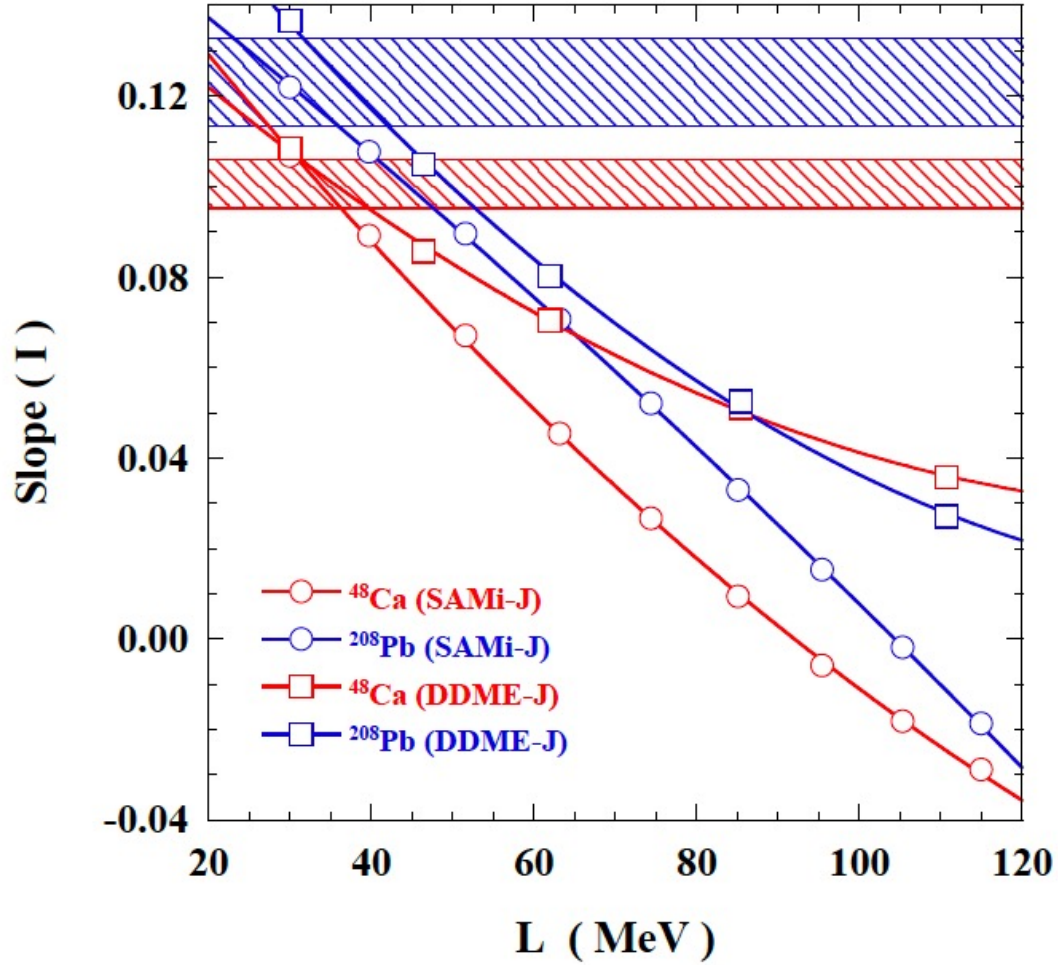

FIG. 22. (color on line) The same as Fig. 21 but for the symmetry energy coefficient L.

Constraints on J and L

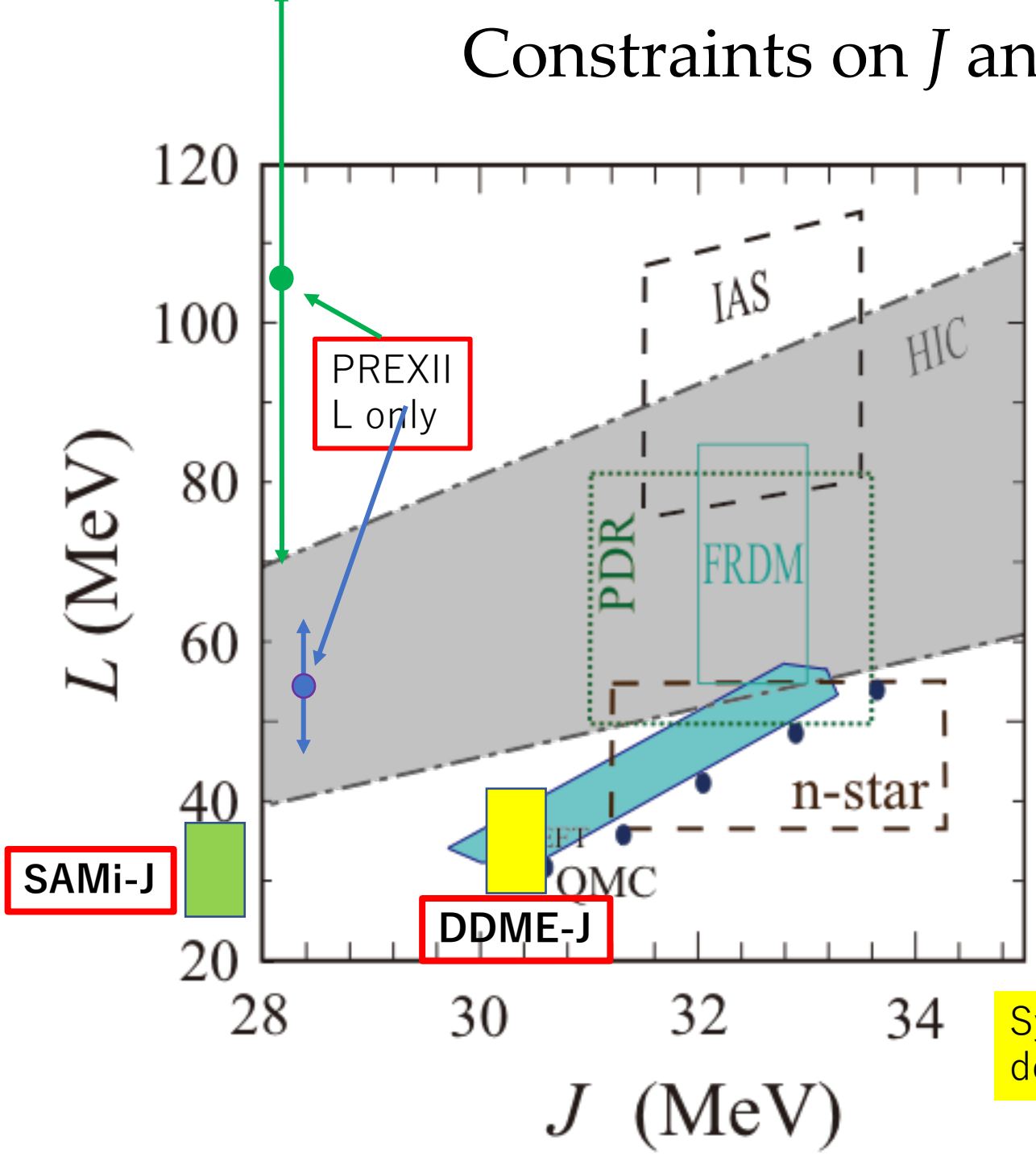

Tsang PRC2012

HIC: Heavy Ion Collision Analysis
Tsang PRL2009

IAS: Isobaric Analog State Energy
Danielewicz&Lee NPA2009

PDR: Pygmy Dipole Resonance in ^{132}Sn, ^{68}Ni, Carbone PRC2010

FRDM: Finite Range Droplet Model
Moeller PRL2012

n-star: Quiescent Low-Mass X-ray Binaries, Stainer PRL2012

χEFT: Chiral Effective Field Theory,
Tews PRL2013

QMC: Quantum Monte-Carlo Calc.
Gandolfi, EPJA50, 10(2014).

Symmetry energy coefficients at low density 0.1 fm^{-3}

Isospin Breaking interactions

Coulomb interaction

Charge symmetry breaking (CSB) interaction

$V_{nn} \neq V_{pp}$

Charge Independence breaking (CIB) interaction

$V_{np} \neq (V_{nn} + V_{pp})/2$

Origin: explicit chiral symmetry breaking

$m_u \neq m_d$

Nucleon and Pion mass difference

Skyrme type ISB interactions

$$v_{\mathrm{Sky}}^{\mathrm{CSB}}(\vec{r}) = s_0(1 + y_0 P_\sigma)\,\delta(\vec{r})\,\frac{\tau_{z1} + \tau_{z2}}{4},$$

$$v_{\mathrm{Sky}}^{\mathrm{CIB}}(\vec{r}) = u_0(1 + z_0 P_\sigma)\,\delta(\vec{r})\,\frac{\tau_{z1}\tau_{z2}}{2}.$$

Energy density functionals

$$\mathcal{E}_{\mathrm{CSB}} = \frac{s_0(1 - y_0)}{8}\left(\rho_n^2 - \rho_p^2\right),$$

$$\mathcal{E}_{\mathrm{CIB}} = \frac{u_0}{8}\left[\left(1 - \frac{z_0}{2}\right)\left(\rho_n + \rho_p\right)^2 - 2(2 + z_0)\rho_n\rho_p\right].$$

Observables

Nolen-Schiffer anomaly,
IAS,
mass differences in isobar and isotriplet nuclei

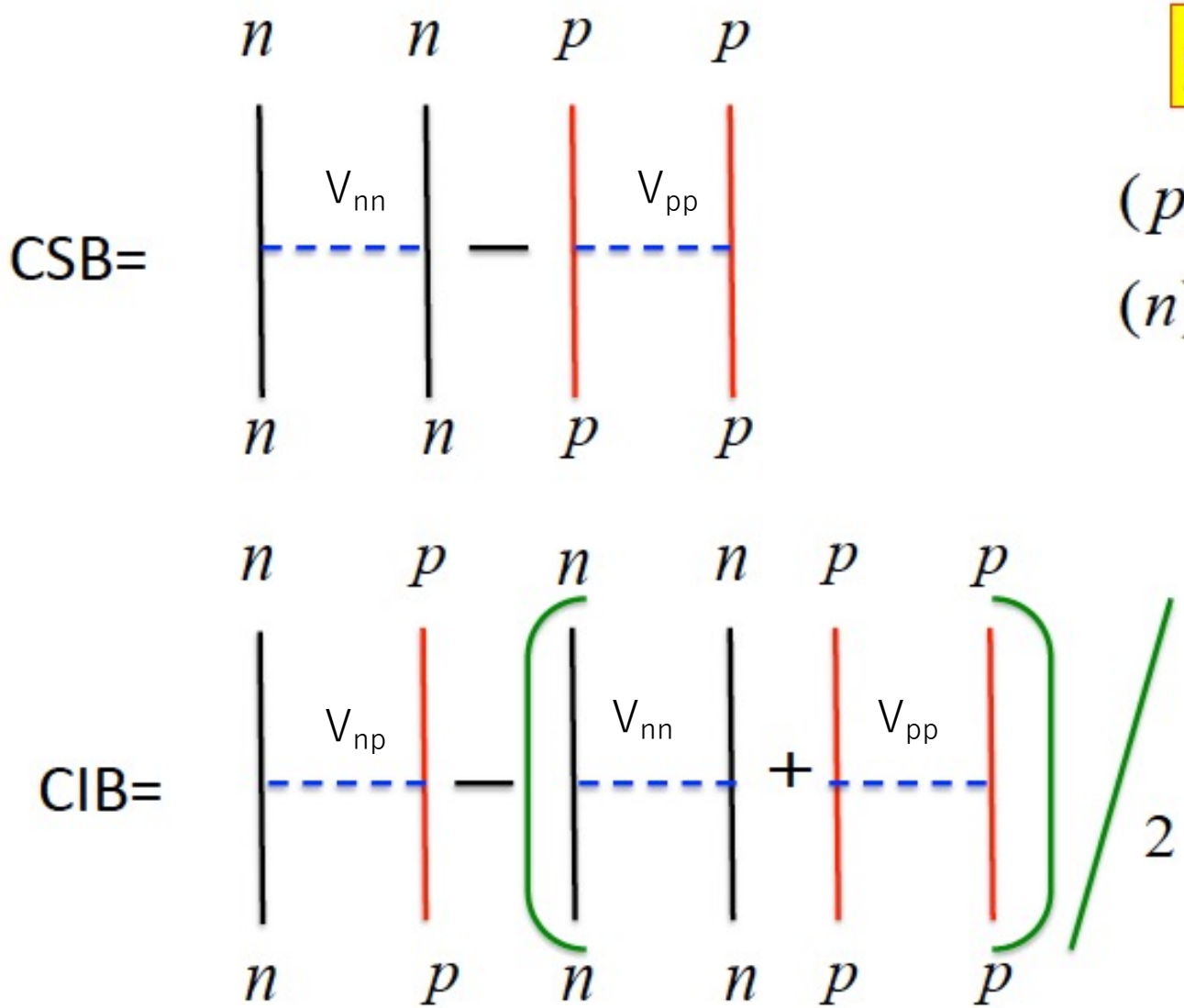

Explicit chiral symmetry breaking effect!

$\rho_{IV} = \rho_n - \rho_p$

Particle-Vibration coupling model (PVC) to IV GMR

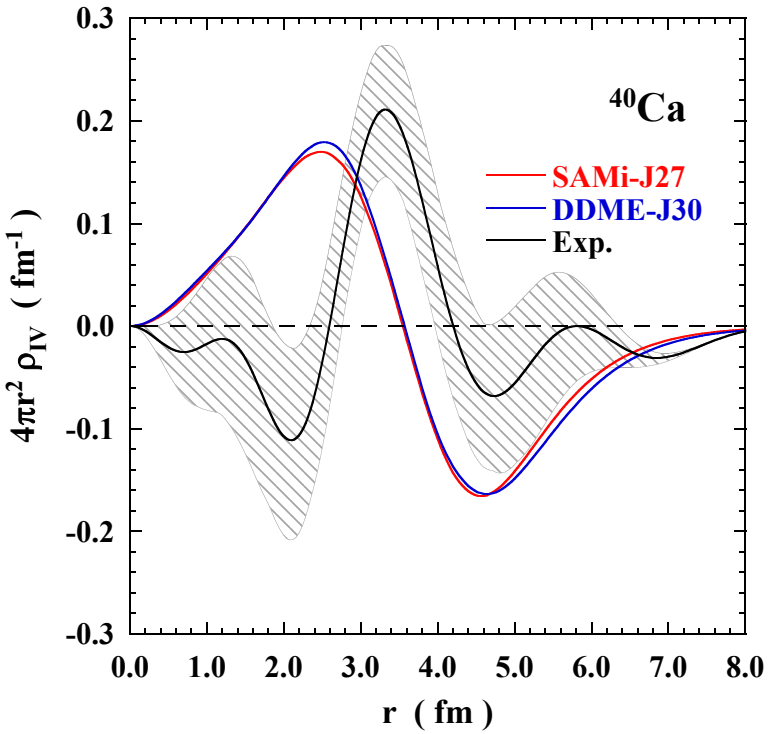

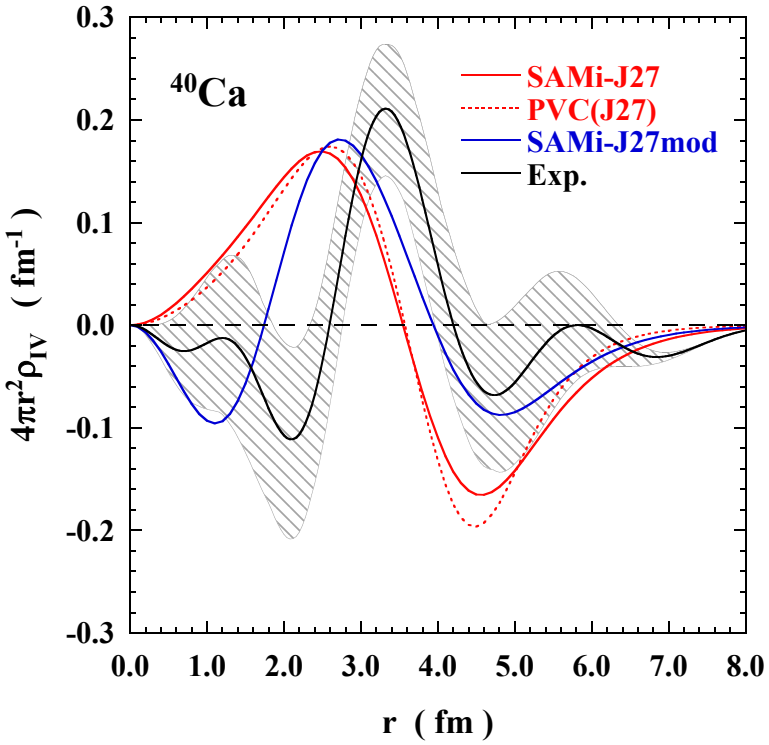

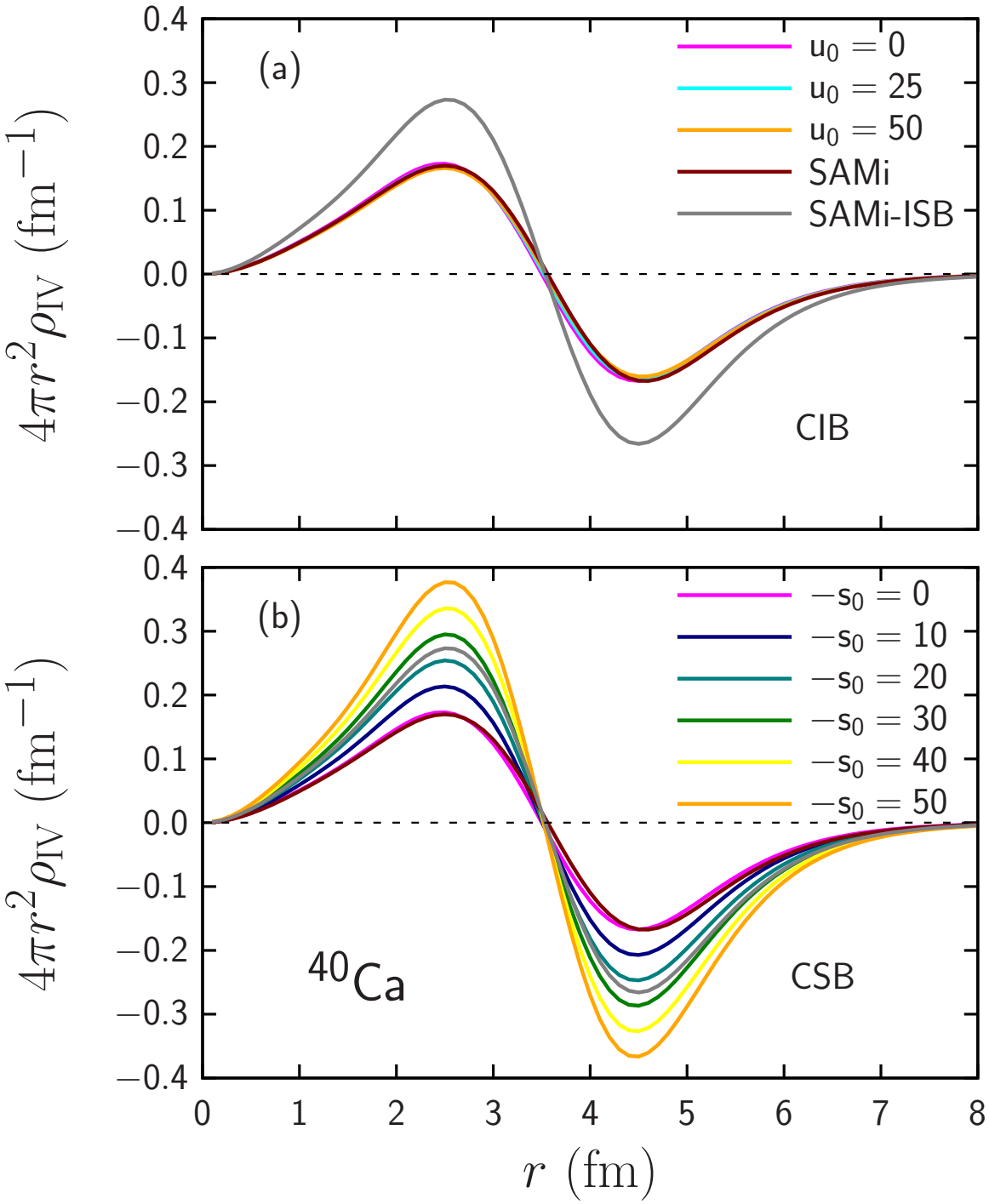

No CIB dependence

SAMi: no ISB
SAMi-ISB:
s_0= -26.3 MeV fm^3
u_0=+25.8 MeV fm^3

A strong CSB dependence

HS et al.,
Physics Letters B829 137072 (April, 2022)

$$\left|\widetilde{\mathrm{GS}}\right\rangle \simeq |\mathrm{GS}\rangle + \varepsilon^{\tau=1} |\mathrm{GMR}, \tau = 1\rangle , \qquad (1)$$

taking into account the coupling between the ground state and the collective IV GMR. Here, $\tau = 1$ denotes the IV GMR. The coefficient $\varepsilon^{\tau=1}$ of the perturbed state is calculated as

$$\varepsilon^{\tau=1} = \frac{\left\langle \mathrm{GMR}, \tau = 1 \middle| V^{\mathrm{ISB}} \middle| \mathrm{GS} \right\rangle}{\Delta E^{\tau=1}}, \qquad (2)$$

Bohr-Mottelson Model

$$\varepsilon(two - fluid)^2 = 3.50 \times 10^{-7} Z^2 A^{2/3}.$$

$\varepsilon^2 \sim 0.2$ %

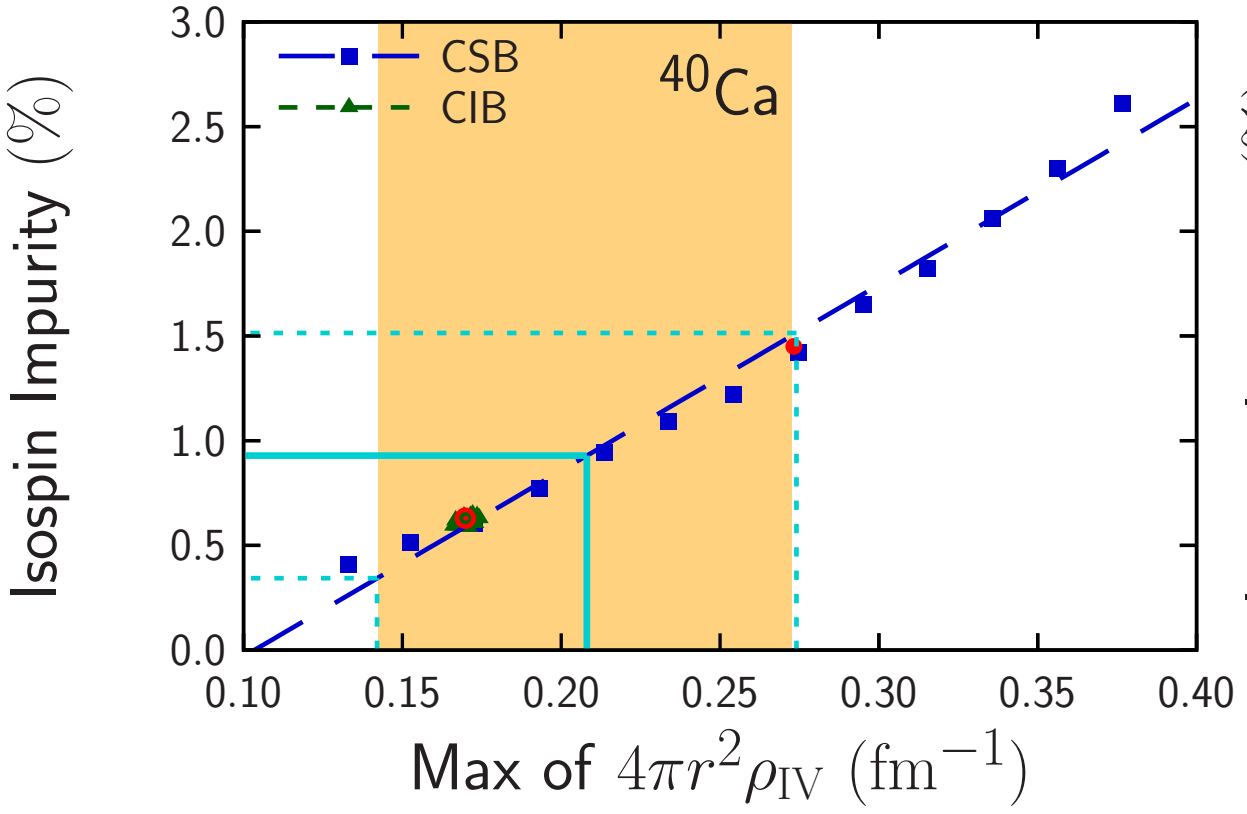

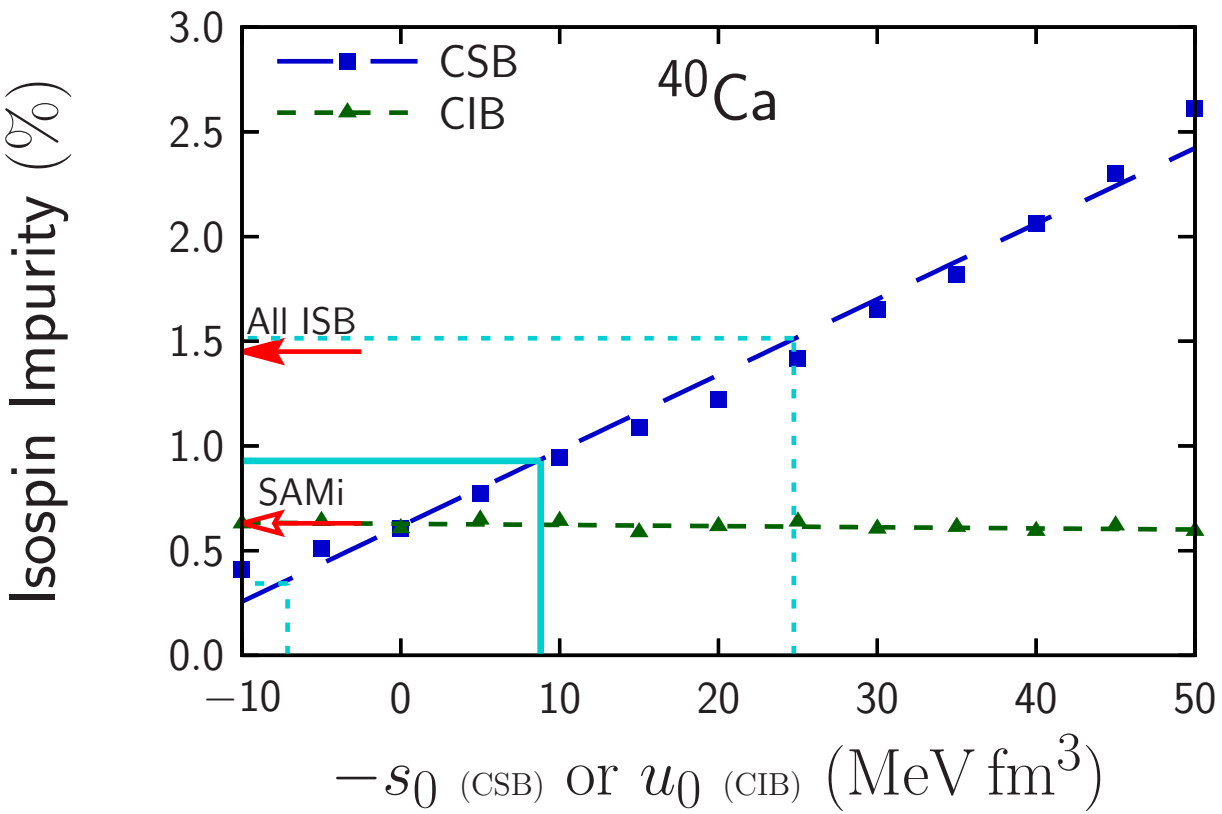

Isospin impurity $\varepsilon^2 = 0.928 \pm 0.586.$ %

CSB interaction $s_0 = -(8.80 \pm 16.0)$ MeV fm^3,

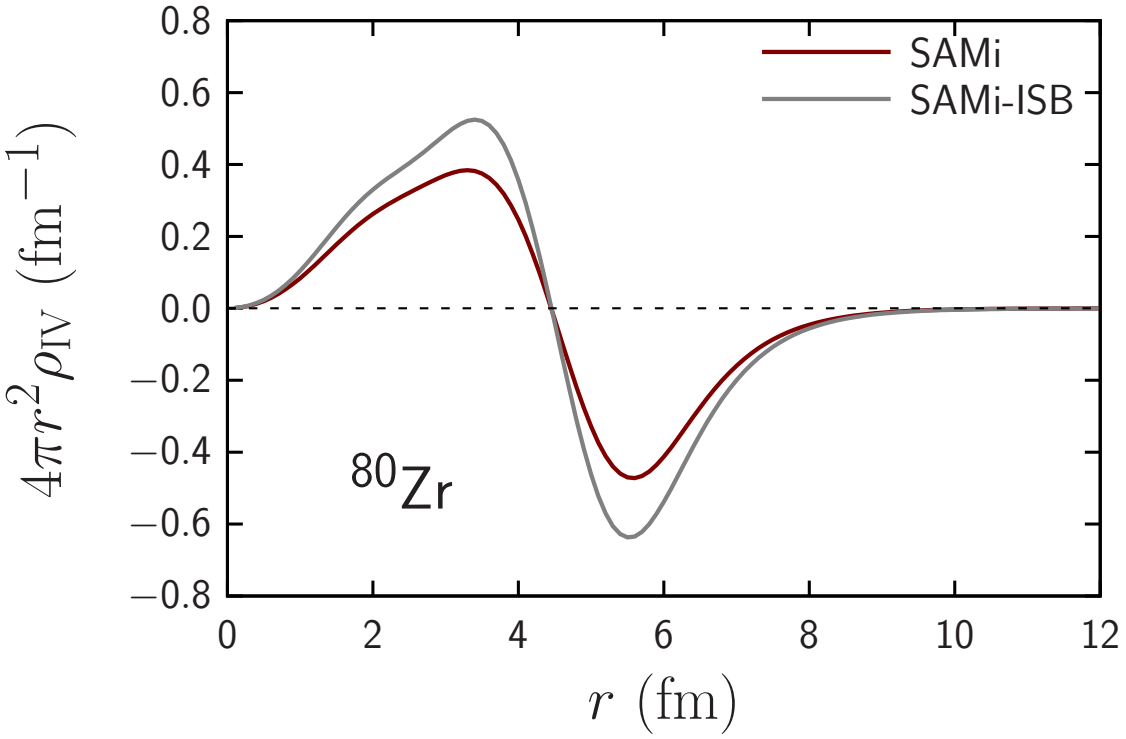
SAMi
SAMi-ISB
^{80}Zr
$4\pi r^2 \rho_{\rm IV}$ (fm^{-1})
r (fm)

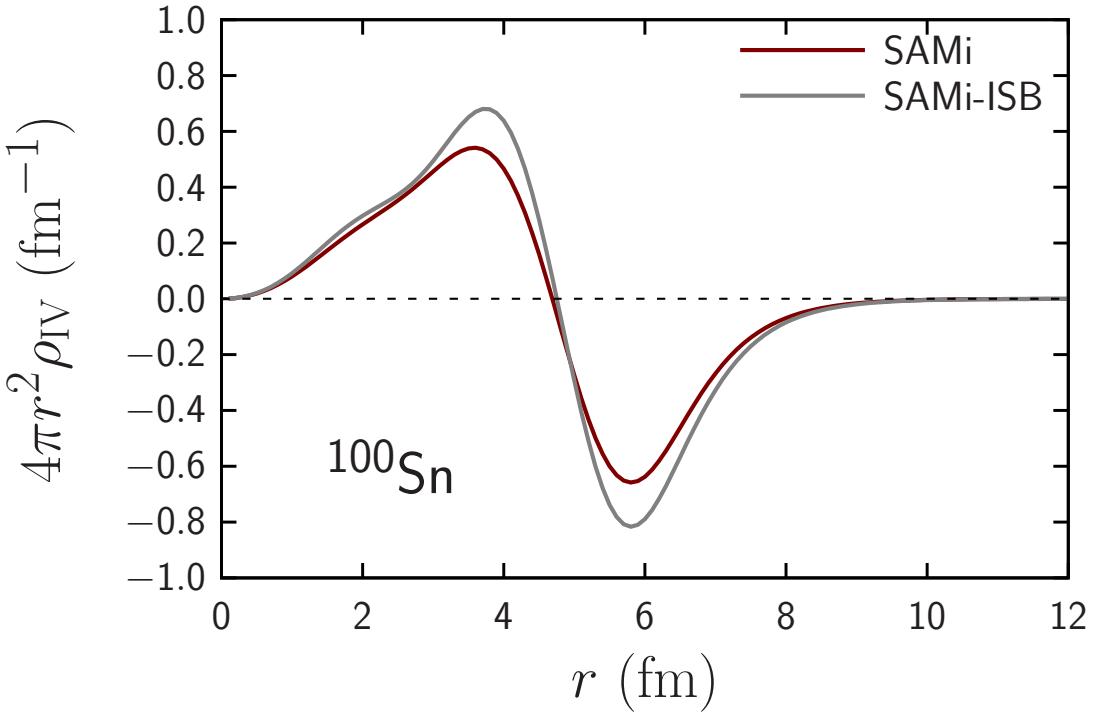
SAMi
SAMi-ISB
^{100}Sn
$4\pi r^2 \rho_{\rm IV}$ (fm^{-1})
r (fm)

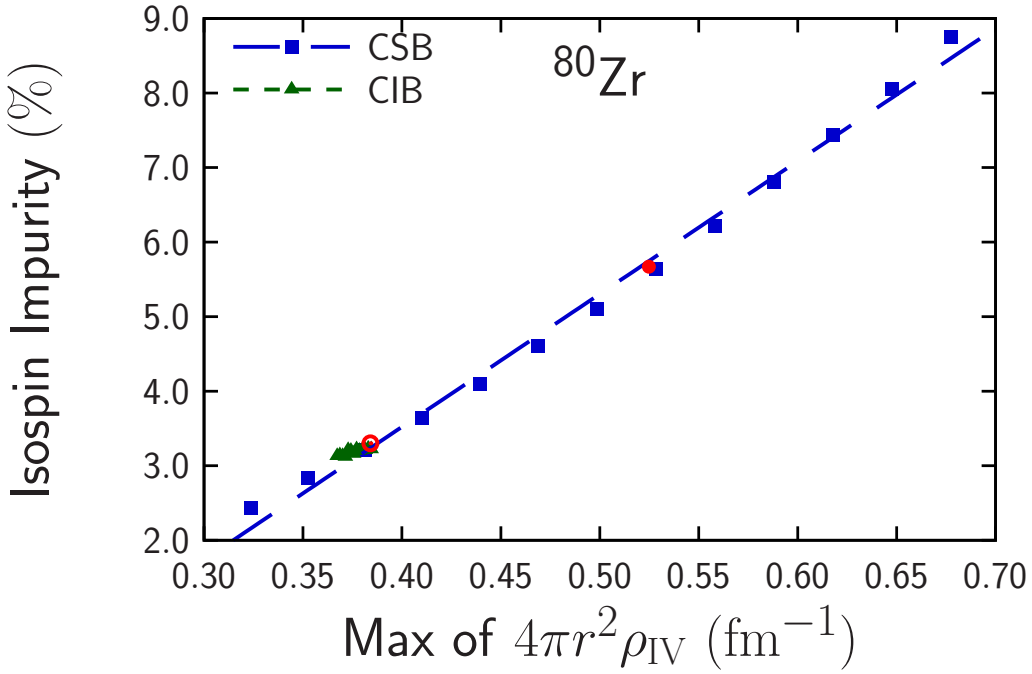
CSB
CIB
^{80}Zr
Isospin Impurity (%)
Max of $4\pi r^2 \rho_{\rm IV}$ (fm^{-1})

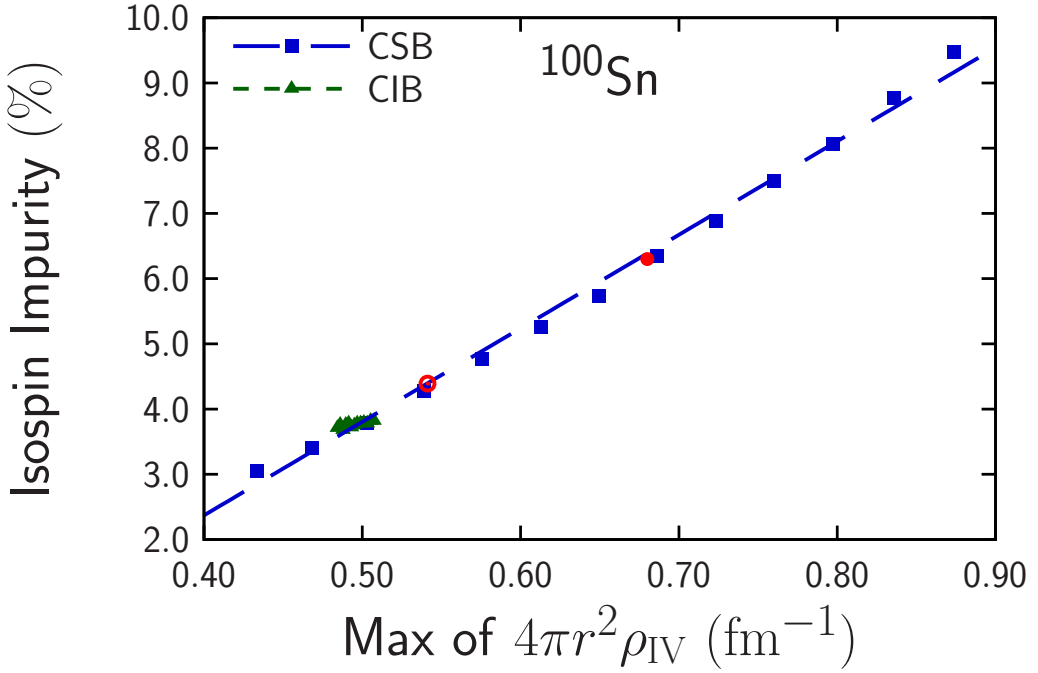
CSB
CIB
^{100}Sn
Isospin Impurity (%)
Max of $4\pi r^2 \rho_{\rm IV}$ (fm^{-1})

Summary of Part 1

the empirical symmetry energy coefficients as

$$J(\mathrm{SAMi-J}) = 27.2 \pm 0.4\ \mathrm{MeV},$$
$$J(\mathrm{DDME-J}) = 30.8 \pm 0.6\ \mathrm{MeV},$$

where we found the difference between the RMF and Skyrme models. For L and K_τ, the two models give very consistent values,

$$L(\mathrm{SAMi-J}) = 31.6 \pm 7.0\ \mathrm{MeV},$$
$$L(\mathrm{DDME-J}) = 36.0 \pm 5.0\ \mathrm{MeV},$$

and

$$K_\tau(\mathrm{SAMi-J}) = -301. \pm 10.\ \mathrm{MeV},$$
$$K_\tau(\mathrm{DDME-J}) = -312. \pm 50.\ \mathrm{MeV}.$$

Symmetry energy coefficients at low density 0.1 fm^{-3}

Summary of Second part

IV density ⇔ Symmetry energy No!
⇔ CIB interaction No!
⇔ CSB interaction Yes!

Future perspectives

^{80}Zr and ^{100}Sn will show more enhanced Isospin breaking effect in the IV density

Collaborators: S. Yoshida (Hosei), T. Naito (iTEMS, RIKEN), T. Suzuki(Nihon University)
T. Uesaka (RIBF,RIKEN), J. Zenihiro (Kyoto), J. Tanaka (RIBF,RIKEN), F. Minato (JAEA)

Thank you very much for your participation!